Preferential HDAC6 inhibitors derived from HPOB exhibit synergistic antileukemia activity in combination with decitabine

Maik Tretbar,[✧,a] Julian Schliehe-Diecks,[✧,b] Lukas von Bredow,[a] Kathrin Tan,[c] Martin Roatsch,[a] Jia-Wey Tu[b], Marie Kemkes,[b] Melf Sönnichsen,[b] Andrea Schöler,[a] Arndt Borkhardt,[b] Sanil Bhatia,[,b] and Finn K. Hansen[*,c¶]*

[✧] *M.T. and J.S.-D. share the first authorship*

* *S.B. and F.K.H. share the senior and corresponding authorship*

[a] Institute for Drug Discovery, Medical Faculty, Leipzig University, Brüderstraße 34, 04103 Leipzig, Germany.

[b] Department of Pediatric Oncology, Hematology and Clinical Immunology, Medical Faculty, Heinrich Heine University Düsseldorf, Moorenstr. 5, 40225 Düsseldorf, Germany.

[c] Department of Pharmaceutical and Cell Biological Chemistry, Pharmaceutical Institute, University of Bonn, An der Immenburg 4, 53121 Bonn, Germany.

* Corresponding authors:

Prof. Dr. Finn K. Hansen, Pharmaceutical and Cell Biological Chemistry, Pharmaceutical Institute, University of Bonn, An der Immenburg 4, 53121 Bonn, Germany. Tel.: (+49) 228 73 5213. Fax: (+49) 228 73 7929. E-mail: finn.hansen@uni-bonn.de.

Dr. Sanil Bhatia, Department of Pediatric Oncology, Hematology and Clinical Immunology, Medical Faculty, Heinrich Heine University Düsseldorf, Moorenstr. 5, 40225 Düsseldorf, Germany. Tel.: (+49) 211 81 04896. Fax: (+49) 211 81 16436. E-mail: sanil.bhatia@med.uni-duesseldorf.de.

Abstract

Histone deacetylase 6 (HDAC6) is an emerging drug target to treat oncological and non-oncological conditions. Since highly selective HDAC6 inhibitors display limited anticancer activity when used as single agent, they usually require combination therapies with other chemotherapeutics. In this work, we synthesized a mini library of analogues of the preferential HDAC6 inhibitor HPOB in only two steps *via* an Ugi four-component reaction as the key step. Biochemical HDAC inhibition and cell viability assays led to the identification of **1g** (highest antileukemic activity) and **2b** (highest HDAC6 inhibition) as hit compounds. In subsequent combination screens, both **1g** and especially **2b** showed synergy with DNA methyltransferase inhibitor decitabine in acute myeloid leukemia (AML). Our findings highlight the potential of combining HDAC6 inhibitors with DNA methyltransferase inhibitors as a strategy to improve AML treatment outcomes.

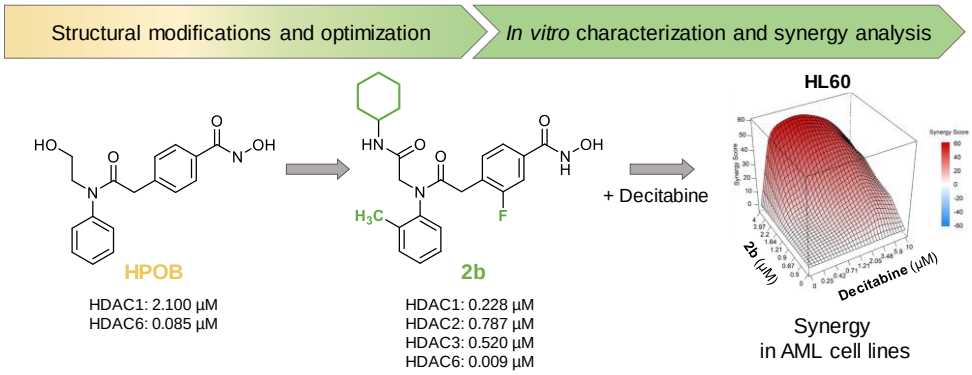

Keywords

Histone deacetylases, HDAC inhibitors, leukemia, cancer, epigenetics

Abbreviations

ACN: acetonitrile; AML: acute myeloid leukemia; $CDCl_3$: chloroform-*d*; CH: cyclohexane; DMSO: dimethylsulfoxide; DNMT: DNA methyltransferase; DNMTi(s): DNA methyltransferase inhibitor(s); EtOAc: ethyl acetate; FDA: U.S. Food and Drug Administration; h: hour(s); HDAC(s): histone deacetylase(s); HDACi: histone deacetylase inhibitor(s); HAT(s): histone acetyltransferase(s); HPOB: *N*-Hydroxy-4-(2-[(2-hydroxyethyl)(phenyl)amino]-2-oxoethyl)benzamide; HSP90: heat shock protein 90; NAD^+: nicotinamide adenine dinucleotide; SI: selectivity index; TFA: trifluoroacetic acid; TLC: thin layer chromatography; U-4CR: Ugi four-component reaction; ZBG(s): zinc-binding group(s);

1. Introduction

Histone deacetylases (HDACs), a class of enzymes, remove acetyl residues from the terminal *N*-acetyl lysine of histones, causing the DNA to wrap more tightly around its histone core.[1] Along with their counterpart, the histone acetyltransferases (HATs), they are essential for the regulation gene expression, playing a critical role in cellular functions such as cell cycle progression, cell differentiation, migration, protein activity and stability, and tumorigenesis.[2,3] Furthermore, dysregulation of histone (de)acetylation, one of the most common epigenetic processes in cancer, can impact cell death pathways and DNA damage repair.[4]

HDACs are classified into different groups: class I (HDAC1, 2, 3, and 8), class IIa (HDAC4, 5, 7, and 9), class IIb (HDAC6 and 10), class III (Sirt1-7), and class IV (HDAC11).[5] While class I, IIa, IIb, and IV HDACs are zinc-dependent, class III isoforms, the so-called sirtuins, are nicotinamide adenine dinucleotide (NAD^+)-dependent.[6] Abnormal expression of HDACs has been linked to the occurrence of different malignant tumors, making HDAC inhibitors (HDACi) a focus of intense research.[7] Currently, the FDA has approved four HDAC inhibitors (Figure 1A) for the treatment of multiple myeloma and T-cell lymphoma: romidepsin (Istodax), panobinostat (Farydak), belinostat (Beleodaq), and vorinostat (Zolinza).[7] These drugs share a common three-motif pharmacophore model, featuring a surface recognition cap group, a hydroxamic acid moiety as a zinc-binding group (ZBG), and a linker that connects the two parts.[8,9] The ZBG is essential for chelation of Zn^{2+} in the enzyme's active site, while the linker contains a non-polar chain or an aromatic ring that allows the cap group to occupy the entrance to the pocket.[10]

HDACs 1-3 and 6 are of particular interest in cancer drug development due to their unique mechanisms of action. HDAC1-3 are often overexpressed in different cancer types, leading to

aberrant gene expression patterns that promote cell survival, proliferation, and resistance to cell death. Inhibitors of HDAC1-3 have shown promising results in preclinical and clinical trials for the treatment of various types of cancer, including lymphoma, leukemia, breast cancer, and lung cancer.[11]

HDAC6 differs from HDAC1-3 in that it predominantly targets non-histone proteins, including α-tubulin, cortactin, STAT3, and HSP90, which are all implicated in cancer development, progression, and metastasis.[12,13] While selective HDAC6 inhibitors have shown promising activity in combination with other therapies like chemotherapy and immunotherapy, their anticancer activity is limited when used alone.[14,15] There is growing evidence suggesting that the anticancer effects of certain HDAC6 inhibitors with anticancer activity are achieved by inhibiting multiple HDAC isozymes including HDAC1-3.[14] As a result, HDAC6 preferential inhibitors like ricolinostat (Figure 1B) and citarinostat, which retain some ability to inhibit HDAC1-3, have shown the most promising activities at the preclinical stage and in clinical trials. *N*-Hydroxy-4-(2-[(2-hydroxyethyl)(phenyl)amino]-2-oxoethyl)benzamide (HPOB, Figure 1B)) is an HDAC6 preferential inhibitor that exhibits 25-fold greater selectivity for HDAC6 over HDAC1 in biochemical HDAC inhibition assays.[16] While it shows inhibitory activity against HDAC6 (IC_{50}: 0.085 μM), it is somewhat less potent than other preferential HDAC6 inhibitors such as ricolinostat or nexturastat A (see Figure 1B).

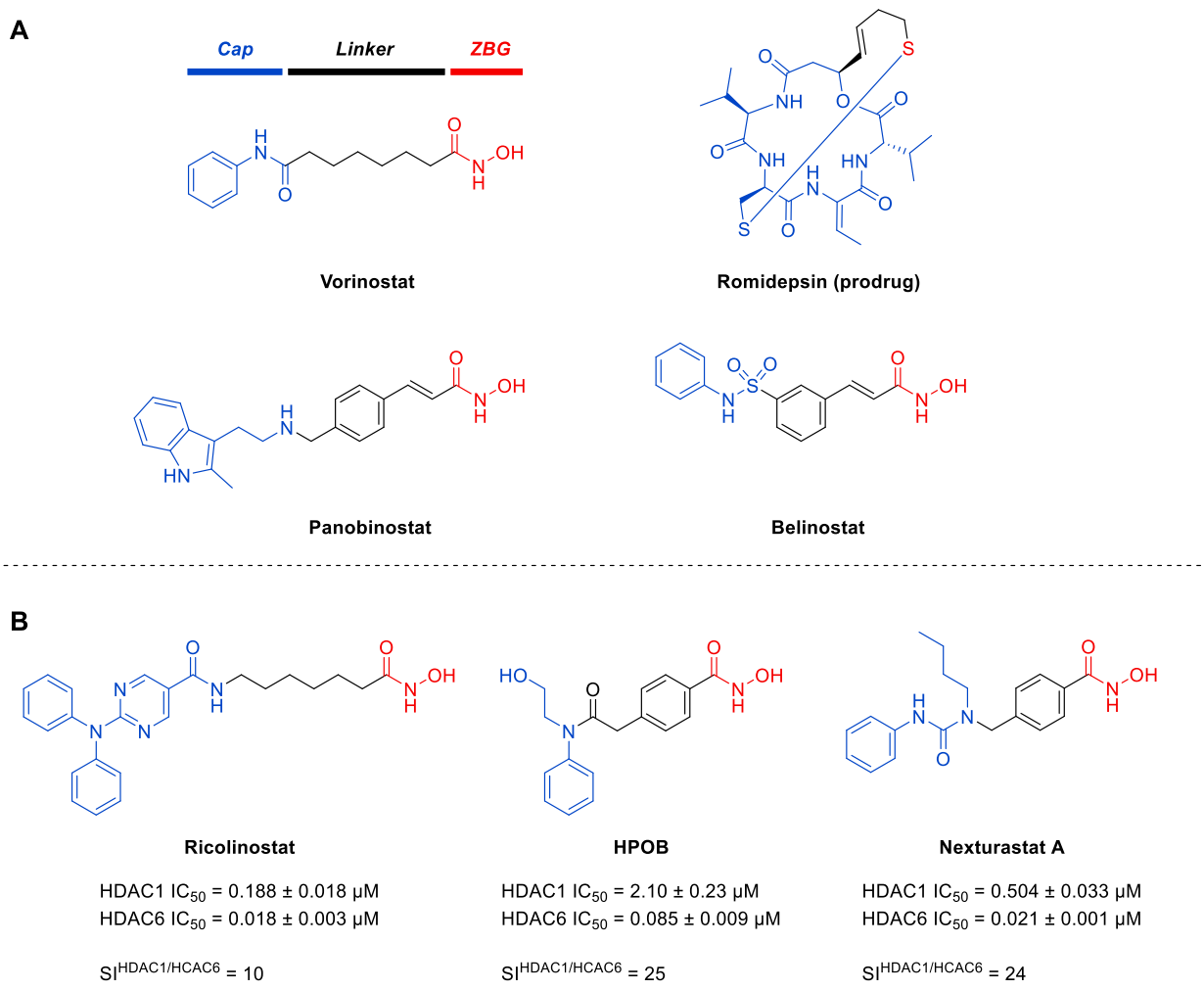

Figure 1. A) Structures of FDA-approved HDACi: vorinostat, romidepsin, belinostat, and panobinostat. B) Selected HDAC6 preferential HDACi with IC_{50} values against HDAC1 and 6. SI = selectivity index. Data from refs[16–18].

Here we aimed to optimize the HDAC inhibitory properties and anticancer activity of HPOB. To expand the structure-activity relationships of this type of HDACi, we synthesized a series of compounds using the Ugi four-component reaction (U-4CR) as a key step, followed by post-Ugi transformations to introduce the hydroxamic acid ZBG. We then evaluated all synthesized

compounds for inhibitory properties against HDAC1 and HDAC6, as well as their antiproliferative activity in three leukemia cell lines. The most promising compounds were then screened for their ability to induce apoptosis and synergistic anticancer activity with the DNA methyltransferase inhibitor decitabine.

2. Results and discussion

2.1. Design and multicomponent synthesis of HPOB analogues

HPOB is a preferential HDAC6 inhibitor utilizing an aromatic linker and a branched cap group. This design principle is well-established to achieve HDAC6 preferential or even selective inhibition and was similarly utilized in frequently used tool compounds such as nexturastat A.[19,20] However, compared to nexturastat A, HPOB demonstrates a reduced inhibitory potency against HDAC6. Consequently, our aim was to improve the HDAC6 inhibition. To this end, we replaced the hydroxylethyl substituent by a substituted acetamide group while retaining the anilide moiety (type **1**, Figure 2). Compounds of this type should be easily accessible by the U-4CR as the key step, thereby enabling the rapid access to a focused library of HPOB analogues. Recently, we and others reported the beneficial effect of linker fluorination in the *meta*-position to the hydroxamic acid on the HDAC6 selectivity profile.[12,21–23] Thus, we also included a series of fluorinated derivatives in our compound design (type **2**, Figure 2).

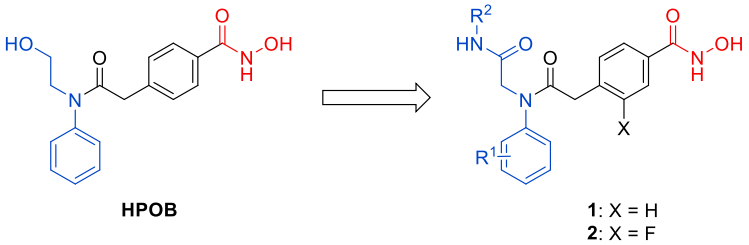

Figure 2. Design of HPOB analogues.

The designed compounds were synthesized in only two steps *via* an U-4CR as key step followed by a hydroxylaminolysis reaction to install the hydroxamic acid as ZBG. In detail, the U-4CR of the respective aniline of type **3**, formaldehyde (**4**) (obtained from paraformaldehyde), the respective carboxylic acid **5** or **6**, and the respective isocyanide **7**, generated the intermediates **8a-i** and **9a-d** within less than 2 hours of microwave irradiation (Scheme 1). After purification of the intermediates, the esters **8a-i** and **9a-d** were treated with a mixture of sodium hydroxide and aqueous hydroxylamine to afford the HPOB analogues **1a-i** and **2a-d**. All final compounds were purified by precipitation from the aqueous crude mixture and subsequent washing steps, column chromatography, or preparative HPLC and exceeded 95% purity.

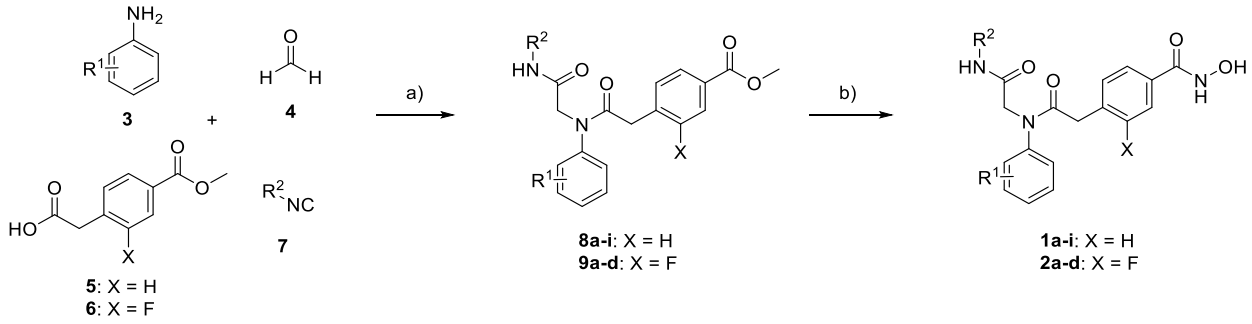

Scheme 1. Microwave-assisted Ugi four-component reaction to synthesize the HPOB analogues **1a-i** and **2a-d**. *Reagents and conditions*: a) (i) **3,** paraformaldehyde, MeOH, Et_3N, 150 W, 45 °C, 30 min; (ii) **5** or **6**, R^2-NC (**7**), 150 W, 45 °C, 1-2 h; b) MeOH, CH_2Cl_2, aq. H_2NOH, NaOH, rt, 2-4 h.

2.2. Inhibition of HDAC1 and HDAC6

The synthesized HPOB analogues **1a-i** and **2a-d** were first tested in fluorogenic assays for their inhibitory potencies against HDAC1 and HDAC6 using HPOB and vorinostat as control compounds. The results are presented in Table 1. HPOB displayed an IC_{50} value of 0.085 µM in combination with a 25-fold selectivity in comparison to HDAC1 ($SI^{HDAC1/6} = 25$). As expected, vorinostat demonstrated a slightly more potent, but unselective inhibition of HDAC6 (HDAC6 $IC_{50} = 0.048$ µM; $SI^{HDAC1/6} = 2$).

In a first set of compounds (**1a-d**) we utilized aniline as amine component and four commercially available isocyanides (cyclohexyl, benzyl, *n*-butyl, and *tert*-butyl) in the U-4CR. Compound **1a** containing a cyclohexyl moiety in the isocyanide region emerged as the most promising compound (HDAC6 $IC_{50} = 0.035$ µM; $SI^{HDAC1/6} = 8$). Consequently, we focused on compounds derived from cyclohexyl isocyanide and modified the aniline part of the HDACi by introducing a methyl group in the *ortho*-, *meta*-, or *para*-position (compounds **1e-g**). The introduction of a methyl group in *ortho*-position (**1e**) led to a 2-fold increase in HDAC6 inhibitory potency compared to **1a** while the selectivity profile was retained (HDAC6 $IC_{50} = 0.017$ µM; $SI^{HDAC1/6} = 8$). In contrast, when the methyl group was inserted into the *meta*-position (**1f**), we noticed a slightly reduced HDAC6 inhibition and selectivity (HDAC6 $IC_{50} = 0.050$ µM; $SI^{HDAC1/6} = 6$). In the case of the *para*-substituted derivative **1g**, a reduced HDAC6 preference was observed (HDAC6 $IC_{50} = 0.041$ µM; $SI^{HDAC1/6} = 2$), leading to a vorinostat-like HDAC inhibition profile.

Due to the promising HDAC6 inhibitory activity of **1e**, we prepared additional compounds with altered residues in the *ortho*-position. The introduction of an ethyl substitution led to a reduced HDAC6 inhibition (compound **1h**, HDAC6 $IC_{50} = 0.035$ µM; $SI^{HDAC1/6} = 10$), while the replacement of the methyl in **1e** by a trifluoromethyl group resulted in similar HDAC6 inhibition

in combination with slightly increased selectivity (compound **1i**, HDAC6 IC_{50} = 0.021 µM; $SI^{HDAC1/6}$ = 11).

Next, we investigated a series of fluorinated analogues of **1a**, **1e**, **1h**, and **1i**. The unsubstituted aniline derivative **2a** (HDAC6 IC_{50} = 0.016 µM; $SI^{HDAC1/6}$ = 22) displayed a 2-fold increased HDAC6 inhibition and ~3-fold improved selectivity compared to its non-fluorinated counterpart **1a**. Since the introduction of a methyl group in the *ortho*-position turned out to be beneficial in the nonfluorinated series, we also studied methyl (**2b**), ethyl (**2c**), and trifluoromethyl (**2d**) derivatives of **2a**. All three compounds showed potent (IC_{50} values ranging from 0.009 to 0.018 µM) and preferential HDAC6 inhibition. Overall, compound **2b** (HDAC6 IC_{50} = 0.009 µM; $SI^{HDAC1/6}$ = 25) emerged as the most potent and selective HDAC6 inhibitor from this series. To conclude, all synthesized HPOB analogues exceeded the HDAC6 inhibitory capacity of HPOB with IC_{50} values ranging from 0.009 to 0.060 µM, albeit with different selectivity profiles ranging from vorinostat-like to HPOB-like.

Table 1. IC_{50} values of nonfluorinated HDACi **1a-i** and fluorinated analogues **2a-d** in comparison to those of HPOB and vorinostat against HDAC1 and HDAC6.

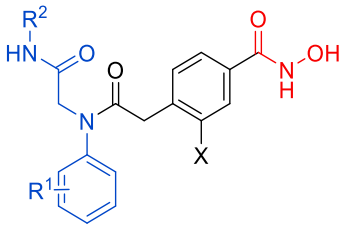

1: X = H
2: X = F

			IC_{50} [µM]		
	R^1	R^2	HDAC1	HDAC6	SI[a]
1a	H	*c*-Hex	0.293 ± 0.033	0.035 ± 0.001	8

1b	H	Bn	0.283 ± 0.001	0.043 ± 0.005	7
1c	H	*n*-Bu	0.450 ± 0.062	0.060 ± 0.006	7
1d	H	*t*-Bu	0.407 ± 0.063	0.059 ± 0.006	7
1e	2-Me	*c*-Hex	0.138 ± 0.008	0.017 ± 0.0004	8
1f	3-Me	*c*-Hex	0.313 ± 0.031	0.050 ± 0.004	6
1g	4-Me	*c*-Hex	0.083 ± 0.001	0.041 ± 0.002	2
1h	2-Et	*c*-Hex	0.363 ± 0.056	0.035 ± 0.004	10
1i	2-CF_3	*c*-Hex	0.230 ± 0.029	0.021 ± 0.004	11
2a	H	*c*-Hex	0.357 ± 0.004	0.016 ± 0.003	22
2b	2-Me	*c*-Hex	0.228 ± 0.035	0.009 ± 0.003	25
2c	2-Et	*c*-Hex	0.275 ± 0.014	0.018 ± 0.002	16
2d	2-CF_3	*c*-Hex	0.265 ± 0.024	0.013 ± 0.001	21
HPOB			2.100 ± 0.231	0.085 ± 0.009	25
vorinostat			0.088 ± 0.008	0.048 ± 0.004	2

[a]Selectivity index [SI = (IC_{50} HDAC1)/(IC_{50} HDAC6)].

2.3. Docking studies

Since compound **2b** was found to be the most potent and selective HDAC6 inhibitor in this series, docking studies were performed to investigate a potential binding mode of the inhibitor in the active site of HDAC6 (Figure 3). Co-crystallization of the HDACi HPOB in complex with *Danio rerio* HDAC6 (PDB ID: 5EF7) revealed a coordination of the zinc ion with a monodentate geometry. Only the deprotonated hydroxyl group of the hydroxamate coordinates the zinc without displacing the zinc-bound water molecule. Additionally, many selective HDAC6 inhibitors bearing bulky and rigid capping groups exhibit this unusual binding mode.[20,24,25] Due to the structural similarity of compound **2b** with HPOB and a comparable selectivity for HDAC6, we assumed a similar binding mode of the hydroxamic acid within the active site of HDAC6. Hence, the hydroxamic acid substructure of HPOB from the crystal structure 5EF7 was used as a template for the docking studies to provide a reasonable complexation of the zinc ion. In order to gain an insight into the putative binding mode of **2b** in human HDAC6, the hydroxamic acid scaffold as

well as the zinc-bound water molecule was placed into the crystal structure of human HDAC6 (PDB ID: 5EDU) by structural alignment. The docking solution revealed a pose within HDAC6's active site that partially resembles the binding mode of HPOB. Due to the scaffold constraint, a monodentate coordination of the zinc ion was determined. In addition, the phenyl linker adjacent to the hydroxamate is placed between two aromatic residues F^{680} and F^{620} that could enable π-π interactions within the active site tunnel. For the two parts of the bifurcated cap group a binding mode was predicted that suggest the occupation of the L1 and L2 pockets. The aromatic 2-methylphenyl cap group is orientated towards L1 loop and fits in the hydrophobic pocket, which is formed by the side chains of H^{500} and P^{501}. Compared to HPOB (see Figure S1, Supporting Information), a slightly different direction of the aromatic cap moiety of compound **2b** was predicted, thus leading to a better steric complementarity to the L1 pocket. The other longer hydrophobic cyclohexyl branch lies in the L2 pocket and is surrounded by the amino acids F^{679} and L^{749}. Both amino acids create a favorable hydrophobic environment for the cyclohexane moiety. Although no direct interaction of the branched groups, i.e. acetamide and anilide moiety, could be observed, the high potency of **2b** against HDAC6 could arise from the optimal positioning of the cap groups that fill out the respective L1 and L2 pocket.

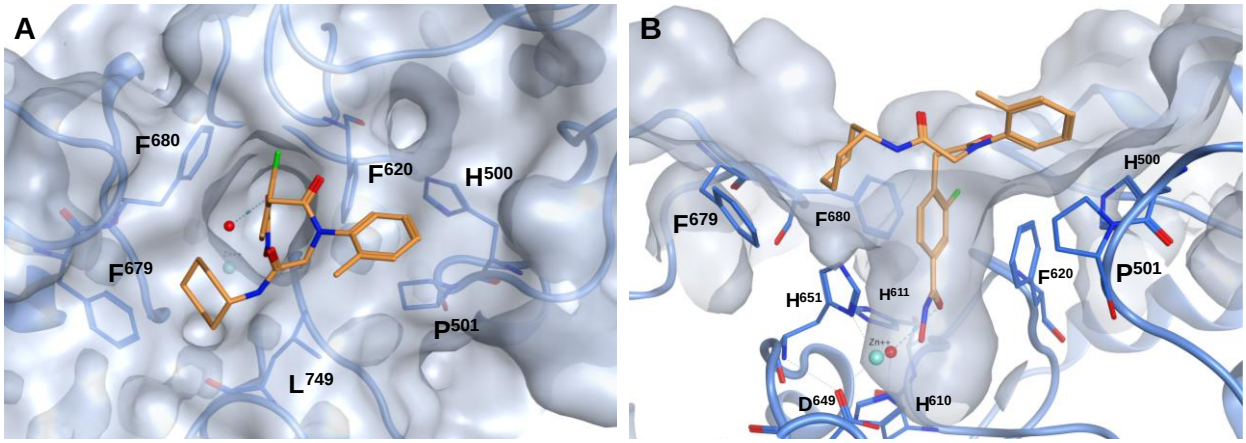

Figure 3. Predicted binding mode of compound **2b** (orange colored) in crystal structure of HDAC6 (PDB ID: 5EDU). A) Top view of the L1 and L2 pocket. B) Side view of the active site. The zinc ion is represented as a cyan sphere. The water molecule is depicted as red sphere.

2.4. Cytotoxicity against leukemia cell lines

All synthesized compounds were next screened for their antiproliferative activity against the three leukemia cell lines HAL01 (B-cell acute lymphoblastic leukemia or B-ALL), HL60 (acute myeloid leukemia or AML), and Jurkat (T-cell acute lymphoblastic leukemia or T-ALL). Vorinostat and HPOB were used as controls; the results are presented in Table 2. Most of the synthesized HPOB analogues exhibited antiproliferative activities in the single digit micromolar range against all three cell lines and thus exceeded the activity of HPOB, which showed double-digit micromolar IC_{50} values. The only exception in this series was compound **1g**, which turned out to be the most potent HPOB analog with a similar cytotoxicity profile as vorinostat and submicromolar IC_{50} values against all three cell lines. Interestingly, both HPOB and **2b** displayed an identical SI for HDAC1/HDAC6 of 25. However, against the three leukemia cell lines, **2b** showed a significant increase in antiproliferative activity, which was more than five times higher than HPOB. This improvement is likely attributable to **2b**'s overall superior HDAC inhibitory properties (see Table 1).

Table 2. Cytotoxicities of nonfluorinated HDACi **1a-i** and fluorinated analogues **2a-d** in comparison to those of HPOB and vorinostat against selected leukemia cell lines.

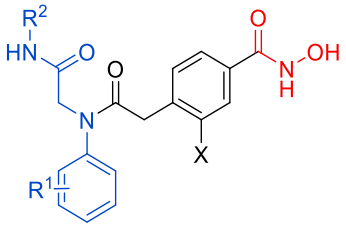

1: X = H
2: X = F

			IC_{50} [µM]		
	R^1	R^2	HAL01	HL60	Jurkat
1a	H	*c*-Hex	2.02 ± 0.44	1.83 ± 0.60	2.54 ± 0.43
1b	H	Bn	2.15 ± 0.77	2.31 ± 0.26	2.29 ± 0.71
1c	H	*n*-Bu	3.12 ± 1.32	2.68 ± 0.81	4.03 ± 1.50
1d	H	*t*-Bu	4.91 ± 1.49	5.99 ± 1.31	8.31 ± 2.85
1e	2-Me	*c*-Hex	1.51 ± 0.31	2.31 ± 0.9	2.52 ± 0.74
1f	3-Me	*c*-Hex	1.89 ± 0.35	1.75 ± 0.99	2.59 ± 0.45
1g	4-Me	*c*-Hex	0.23 ± 0.10	0.36 ± 0.06	0.41 ± 0.06
1h	2-Et	*c*-Hex	1.43 ± 0.12	1.34 ± 0.32	2.28 ± 0.15
1i	2-CF_3	*c*-Hex	3.03 ± 1.17	2.09 ± 1.74	4.58 ± 0.78
2a	H	*c*-Hex	2.08 ± 1.04	1.34 ± 0.56	2.42 ± 0.55
2b	2-Me	*c*-Hex	2.32 ± 0.77	2.04 ± 0.62	3.08 ± 0.59
2c	2-Et	*c*-Hex	1.44 ± 0.29	1.51 ± 0.89	3.21 ± 0.60
2d	2-CF_3	*c*-Hex	1.79 ± 0.26	1.61 ± 0.69	2.28 ± 0.48
HPOB			13.86 ± 3.89	11.33 ± 7.22	16.07 ± 2.52
vorinostat[a]			0.30 ± 0.05	0.22 ± 0.05	0.47 ± 0.02

2.5. Selection of hit compounds and extended HDAC isoform profiling

Based on their antiproliferative activities and HDAC6 inhibition profiles we selected compounds **1g** (highest antileukemia activity) and **2b** (highest and most selective HDAC6 inhibition) for additional experiments. First, we performed an extended HDAC isoform profiling and screened both compounds for their inhibition of HDAC2 and HDAC3 using vorinostat as control; the results are summarized in Table 3. As expected, **1g** emerged as an unselective inhibitor with IC_{50} values of 0.112 and 0.042 µM against HDAC2 and HDAC3, respectively. In contrast, compound **2b** showed even higher selectivity for HDAC6 against HDAC2 (IC_{50} = 0.787 µM; $SI^{HDAC2/6}$ = 87) and HDAC3 (IC_{50} = 0.520 µM; $SI^{HDAC3/6}$ = 58) compared to HDAC1 (IC_{50} = 0.228 µM; $SI^{HDAC1/6}$ = 25).

Table 3. Extended HDAC isoform profiles of **1g** and **2b**.

	IC_{50} [µM]			
	HDAC1	HDAC2	HDAC3	HDAC6
1g	0.083 ± 0.001	0.112 ± 0.004	0.042 ± 0.003	0.042 ± 0.002
2b	0.228 ± 0.035	0.787 ± 0.003	0.520 ± 0.014	0.009 ± 0.003
vorinostat	0.088 ±0.008	0.140 ± 0.019	0.096 ± 0.012	0.048 ± 0.004

*2.6. **1g** and **2b** induce cytotoxicity against leukemia cells via activating apoptosis*

To comprehensively evaluate the antileukemic properties of **1g** and **2b**, we used a high-throughput drug screening approach by employing a diverse panel of leukemia cell lines. Additionally, we included two commercially available inhibitors, CI994 (tacedinaline) and ricolinostat, as positive controls (Figure 4A). Notably, **1g** exhibited superior cytotoxic activity against leukemia cell lines compared to the reference inhibitors, as evidenced by its IC_{50} profile (mean IC_{50} fold change = 6.8 compared to CI994 and 9.7 for ricolinostat). In contrast, **2b** demonstrated comparable IC_{50} values, occasionally surpassing the reference inhibitors in specific cases (mean IC_{50} fold change = 0.95 for CI994 and 1.35 for ricolinostat). Notably, the AML cell lines exhibited comparatively higher susceptibility to both **1g** and **2b**. To assess whether **1g** and **2b** operate within a therapeutic window, avoiding general cytotoxicity against healthy cells, we included healthy fibroblast controls in our screening. Importantly, neither **1g** nor **2b** exhibited any cytotoxic activity against healthy fibroblasts.

Subsequent investigation into markers of HDAC inhibition, such as acetylation levels of H3 (HDAC class I target) and α-tubulin (HDAC6 target) through immunoblotting at various inhibitor concentrations, revealed distinct patterns (Figure 4B). In the case of **1g**, α-tubulin hyperacetylation was relatively weak at lower concentrations, where H3 acetylation levels were significantly increased. When compared, **1g** (24 nM) elicited analogous levels of H3 hyperacetylation at a concentration as low as 2.67% of that required for ricolinostat (0.9 µM), while causing minimal changes to α-tubulin acetylation. In contrast, as expected, **2b** efficiently increased α-tubulin acetylation while affecting H3 acetylation to a lesser extent, mirroring the effects of ricolinostat at similar compound concentrations.

Subsequent to this, we examined the potential of **1g** and **2b** to induce apoptosis through annexin-PI staining (Figure 4C). Relative to the DMSO control, **1g** demonstrated a substantial reduction in the population of viable cells by half, accompanied by an elevation in the percentages of early, late apoptotic, and dead cells. Conversely, **2b** exhibited less pronounced shifts, yet still exhibited a significant increase in the percentage of late apoptotic cells.

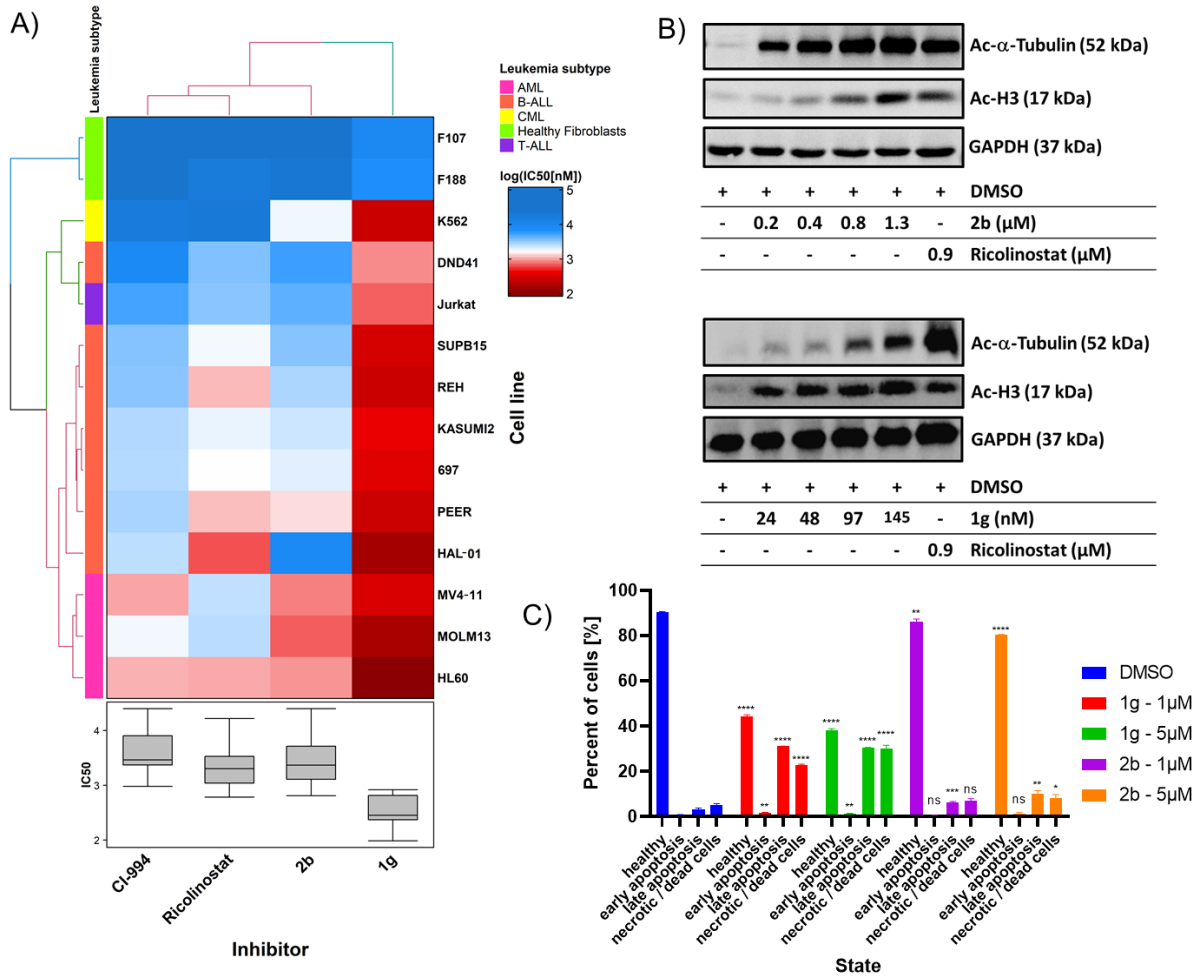

Figure 4. A) Comparative cellular viability (log IC_{50} nM) of different sub-groups of leukemic cell lines (K562, DND41, Jurkat, SUPB15, REH, Kasumi 2, 697, PEER, HAL01, MV4-11, MOLM13 and HL60) and healthy fibroblasts (F107 and F188), after treatment with **1g** and **2b** in comparison to the commercially available selective HDAC6 inhibitors ricolinostat and HDAC class I inhibitor

CI-994 (n = 3). The log IC50 nM data was visualized through a clustered heat map, accompanied by unsupervised hierarchical clustering. The dendrogram represents the similarity between inhibitors, while the color of each tile indicates its position along a gradient of log IC50 (nM). B) Western Blot analysis was performed to evaluate the impact on HDAC inhibition markers, specifically acetylated H3 (ac-H3) and acetylated Tubulin (ac-Tubulin), after a 24-hour treatment with compounds **1g**, **2d**, and the control, ricolinostat, in HL60 leukemia cells (n=3). The presented blot includes a representative sample, with GAPDH employed as the loading control. C) Annexin-PI staining to evaluate the induction of apoptosis in HL60 leukemia cells exposed to **1g** and **2b** at concentrations of 1 µM and 5 µM over a 48-hour period (n=3). The bar graphs displays statistical significance (unpaired t test), * = $p < 0.05$, **= $p < 0.01$, ***= $p < 0.001$, ****= $p < 0.0001$.

*2.7. **1g** and **2b** synergize effectively with the standard chemotherapeutic decitabine against AML cells*

A cornerstone of every modern leukemia treatment protocol is the combination a several anticancer chemotherapeutics. It is crucial that these agents exhibit synergistic interactions to maximize leukemia cell eradication while minimizing cytotoxic side effects. A widely recognized synergistic drug combination includes the use of DNA methyltransferase inhibitors (DNMTis), such as decitabine, in combination with HDAC inhibitors.[12,26,27] To explore the potential synergistic effects of combining **1g** or **2b** with decitabine, we utilized a matrix drug screening approach with the zero interaction potency (ZIP) algorithm (Figure 5). In the case of **2b**, we observed particularly high ZIP synergy scores of around 60 across a broad range of concentrations in both AML cell lines (HL60 and MOLM13; Figure 5A and 5B). Interestingly, in HAL-01 (B-ALL) or JURKAT (T-ALL), no substantial synergy was observed (Figure 5C and 5D). In fact, the drug synergy matrices for HAL-01 and JURKAT displayed a trend towards antagonism,

highlighting the potential selectivity of this synergistic response in the context of AML. When combined with decitabine, **1g** also showed synergistic effects against HL60 and MOLM13 cells, albeit with notably lower ZIP scores (~10-15) than those observed with **2b** (Figures 5E and 5F). This indicates that although **1g** is more potent as an individual cytotoxic inhibitor, **2b** excels significantly in inducing specific drug synergy with decitabine against AML cells.

Consistent with this, a prior study revealed that the combination of a DNMTi and HDAC6 inhibitors can augment anti-tumor immune signaling and reduce tumor burden in ovarian cancer.[28] However, further studies will be required to determine the specific mechanisms contributing to the heightened synergistic interaction observed against AML cells upon combining preferential HDAC6 inhibitors with DNMTi.

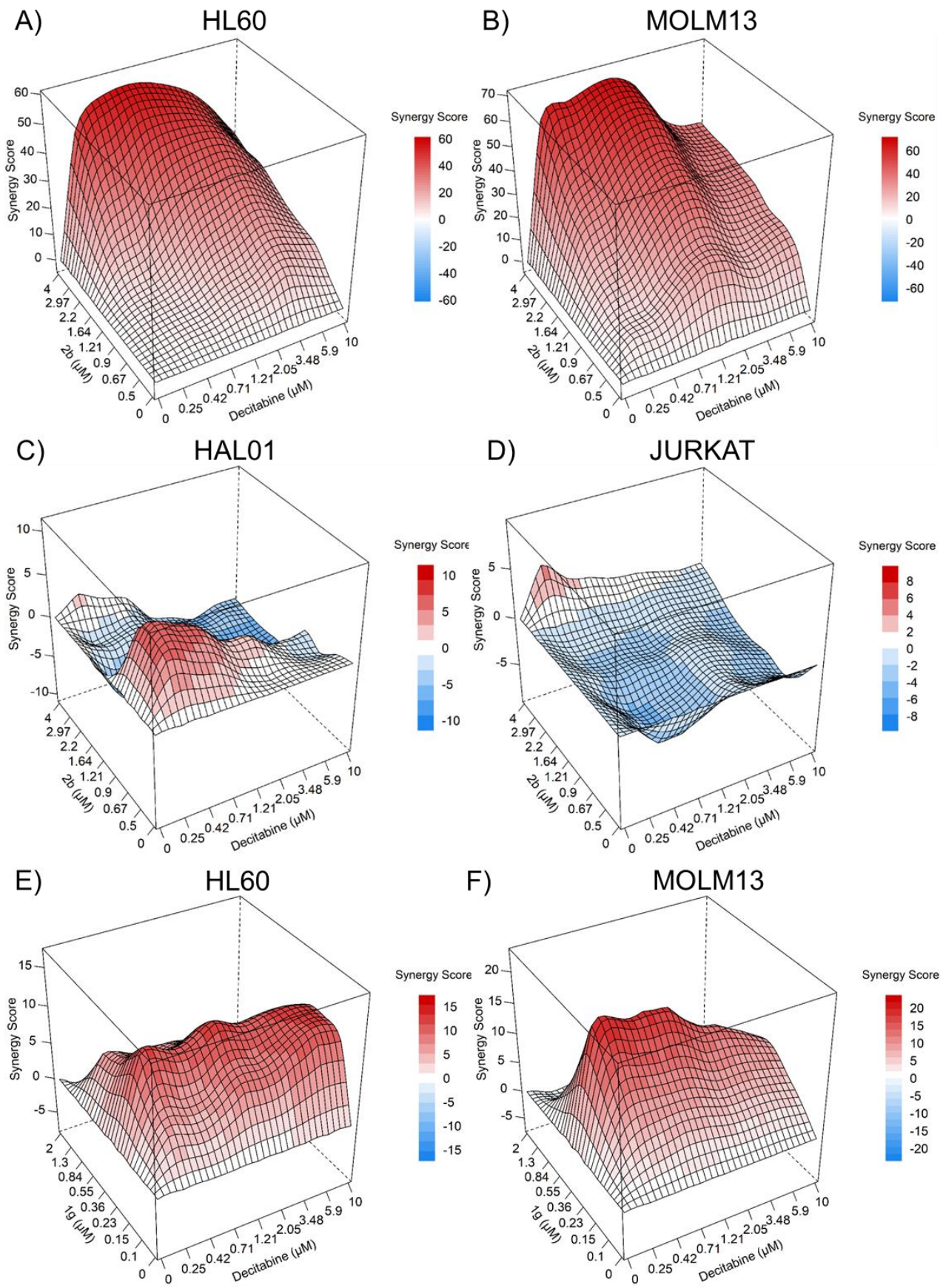

Figure 5. Illustrative synergy plot representing the effects of **2b** after co-treatment of (A) HL60, (B) MOLM13, (C) HAL01 and (D) Jurkat leukemic cell lines with decitabine for 72 hours. Illustrative synergy plot representing the effects **1g** after co-treatment of (E) HL60 and (F) MOLM13 cell lines with decitabine for 72 hours. Synergy scores were calculated using the ZIP model, and visualizations were conducted using the SynergyFinder webtool.[29]

3. Conclusions

In summary, we have synthesized a series of HPOB analogues via a simple and efficient two-step protocol relying on the U-4CR as the key step. The subsequent isoform profiling against HDAC1 and 6 provided important structure-activity relationships. All synthesized analogues of HPOB (0.085 μM) demonstrated superior HDAC6 inhibitory capacities compared to HPOB, exhibiting IC_{50} values ranging from 0.009 to 0.060 μM. However, they displayed different HDAC1 *vs.* HDAC6 selectivity profiles, ranging from vorinostat-like to HPOB-like. In this series, compound **2b** stood out as the most potent and selective HDAC6 inhibitor, with an HDAC6 IC_{50} value of 0.009 μM and a selectivity index ($SI^{HDAC1/6}$) of 25. The subsequent viability assays in three different leukemia cell lines (HAL01, HL60, and Jurkat) led to the identification of **1g** as the compound with the highest antiproliferative activity. Notably, it demonstrated submicromolar activity against all three cell lines. Considering their antiproliferative activities and HDAC6 inhibition profiles, we chose compounds **1g** (due to its highest antileukemia activity) and **2b** (highest and most selective HDAC6 inhibition) for further experiments.

To investigate the antileukemic properties of **1g** and **2b** in more detail, we used a high throughput drug screening approach using a diverse panel of leukemia cell lines. In particular, the AML subcluster was susceptible to HDAC inhibition. Immunoblot analysis conducted on HL60 cells, focusing on histone H3 *vs* α-tubulin hyperacetylation, corroborated the selectivity profiles observed in the biochemical HDAC inhibition assays for compounds **1g** (demonstrating unselective inhibition) and **2b** (exhibiting preferential HDAC6 inhibition). In subsequent combination screenings, both **1g** and, in particular, **2b** exhibited synergy with the DNMTi decitabine in AML cell lines. These findings emphasize the therapeutic promise of combining preferential HDAC6 inhibitors with DNMTis, such as decitabine.

4. Experimental section

4.1. Synthesis

4.1.1. General

All reagents and solvents were purchased from commercial sources and used without further purification. The carboxylic acids **5** and **6** were prepared according to a known procedure.[30] Dry solvents, e.g. MeOH and DCM, were obtained from the MBraun MB SPS-800 solvent purification system. All microwave-assisted reactions were carried out with a CEM Focused Microwave System, Model Discover. Flash column chromatography was performed on silica gel (0.040-0.063 mm, 230-400 mesh, pore size 60 Å) with the solvent mixtures specified in the corresponding experiment. Thin layer chromatography (TLC) was carried out using Macherey-Nagel pre-coated aluminium foil sheets, which were visualised using UV light (254 nm). Hydroxamic acids were stained using a 1 % solution of iron(III) chloride in MeOH. ^{1}H-NMR and ^{13}C-NMR spectra were recorded at room temperature on a Bruker Avance III HD or Varian/Agilent Mercury-plus (300, 400, 500 or 600 MHz) spectrometer using DMSO-d_6 or $CDCl_3$ as solvents. Chemical shifts are given in parts per million (ppm), relative to residual solvent peak for ^{1}H and ^{13}C. Due to the well-known phenomenon of *cis*/*trans*-amide bond rotamers in peptoids,^{1}H and ^{13}C NMR-signals can occur as two distinct sets of signals. Coupling constants (*J*) are reported in Hertz (Hz). Mass-spectra were measured by the Leipzig University Mass Spectrometry Service using electrospray ionisation (ESI) on Bruker Daltonics Impact II and Bruker Daltonics micrOTOF spectrometers. The uncorrected melting points were determined using a Barnstead Electrothermal 9100 apparatus. Analytical HPLC analysis were carried out using a Gynkotek GINA 50 apparatus equipped with a Dionex P680A LPG pump, a Dionex UVD 340 U detector, and a Gina 50 autosampler and a Macherey-Nagel NUCLEODUR 100-5 C_{18} ec columns (250 mm x 4.6 mm). UV absorption was

detected at 254 nm with a linear gradient of 10 % B to 100 % B within 30 min. HPLC-grade water + 0.1 % TFA (solvent A) and HPLC-grade acetonitrile + 0.1 % TFA (solvent B) were used for elution at a flow rate of 1 mL/min. The purity of the final compounds was at least 95.0 %.

4.1.2. Synthesis and compound characterization

*General procedure A for the preparation of UGI compounds **8a-i** and **9a-d**.* In a 10 mL microwave reaction tube, 1.2 equivalents of amine (freshly distilled) and 1.2 equivalents of paraformaldehyde were dissolved in methanol (4 mL). The reaction mixture was irradiated at T = 45 °C and 150 W for 30 minutes. Subsequently, 1.0 equivalent of the carboxylic acid component and 1.0 equivalents of the isocyanide component were added to the turbid white suspension. The reaction mixture was subjected to microwave irradiation at T = 45 °C and 100 W for 1-2 h. The reaction was monitored by thin-layer chromatography and HPLC. The solvent was removed under reduced pressure, washed with aqueous Na_2CO_3 (pH > 7), and extracted with dichloromethane. The desired product was purified by column chromatography (cyclohexane/ethyl acetate as a gradient [4:1] to [1:1]).

*Methyl 4-(2-((2-(cyclohexylamino)-2-oxoethyl)(phenyl)amino)-2-oxoethyl)benzoate **(8a)**.* Synthesized from **5**, cyclohexyl isocyanide (**7a**), paraformaldehyde (**4**), aniline (**3**) according to the general procedure A in 72% yield as a colorless oil: **^{1}H-NMR** ($CDCl_3$, 400 MHz): δ [ppm] = 7.92 (d, J = 8.3 Hz, 2H), 7.46 – 7.30 (m, 3H), 7.20 – 7.14 (m, 2H), 7.12 (d, J = 8.0 Hz, 2H), 6.14 (d, J = 7.9 Hz, 1H), 4.24 (s, 2H), 3.90 (s, 3H), 3.82 – 3.68 (m, 1H), 3.57 (s, 2H), 1.93 – 1.78 (m, 2H), 1.72 – 1.60 (m, 2H), 1.40 – 1.28 (m, 2H), 1.23 – 1.00 (m, 4H). **^{13}C-NMR** ($CDCl_3$, 101 MHz): δ [ppm] = 171.3, 167.8, 167.0, 142.7, 140.3, 130.0, 129.8, 129.1, 128.8, 128.1, 55.4, 52.2, 48.2 41.1, 33.0 (2C), 25.6 (2C), 24.8. HRMS calculated for $C_{24}H_{29}N_2O_4$: 409.2127, found: 409.2129 ($[M+H]^+$), TLC (CH/EtOAc 1/1): R_f = 0.30.

*Methyl 4-(2-((2-(benzylamino)-2-oxoethyl)(phenyl)amino)-2-oxoethyl)benzoate (**8b**).* Synthesized from **5**, benzyl isocyanide (**7b**), paraformaldehyde (**4**), aniline (**3**) according to the general procedure A in 64% yield as a colorless oil: **^{1}H-NMR** ($CDCl_3$, 400 MHz): δ [ppm] = 7.88 (d, *J* = 8.2 Hz, 2H), 7.45 - 7.05 (m, 12H), 6.60 (br. s., 1H), 4.47 (d, *J* = 4.5 Hz, 2H), 4.34 (s, 2H), 3.90 (s, 3H), 3.57 (s, 2H). **^{13}C-NMR** ($CDCl_3$, 101 MHz): δ [ppm] = 171.5, 168.5, 167.0, 142.5, 140.1, 138.1, 130.0, 129.8, 129.2, 128.8, 128.8, 128.1, 127.8, 127.6, 54.4, 52.2, 43.6, 41.0. HRMS calculated for $C_{25}H_{25}N_2O_4$: 417.1814, found: 417.1808 ($[M+H]^+$), TLC (CH/EtOAc 1/1): R_f = 0.30.

*Methyl 4-(2-((2-(butylamino)-2-oxoethyl)(phenyl)amino)-2-oxoethyl)benzoate (**8c**).* Synthesized from **5**, *n*-butyl isocyanide (**7c**), paraformaldehyde (**4**), aniline (**3**) according to the general procedure A in 37 % yield as a yellowish oil: **^{1}H-NMR** ($CDCl_3$, 400 MHz): δ [ppm] = 7.94 (d, *J* = 8.2 Hz, 2H), 7.41 (m, 3H), 7.20 (m, 2H), 7.14 (d, *J* = 8.1 Hz, 2H), 6.27 (br. s, 1H), 4.27 (s, 2H), 3.92 (s, 3H), 3.59 (s, 2H), 3.26 (dd, *J* = 6.9, 13.0 Hz, 2H), 1.46 (dt, *J* = 7.3, 14.8 Hz, 2H), 1.32 (dt, *J* = 6.1, 19.9 Hz, 2H), 0.91 (t, *J* = 7.3 Hz, 3H). **^{13}C-NMR** ($CDCl_3$, 101 MHz): δ [ppm] = 171.4, 168.4, 166.9 142.5, 140.1, 123.0, 129.7, 129.08, 128.8, 128.72, 127.9, 54.5, 52.1, 40.9, 39.3, 31.6, 20.0, 13.7. HRMS calculated for $C_{22}H_{27}N_2O_4$: 383.1971, found: 383.1967 ($[M+H]^+$), TLC (CH/EtOAc 1/1): R_f = 0.24.

*Methyl 4-(2-((2-(tert-butylamino)-2-oxoethyl)(phenyl)amino)-2-oxoethyl)benzoate (**8d**).* Synthesized from **5**, *tert*-butyl isocyanide (**7d**), paraformaldehyde (**4**), aniline (**3**) according to the general procedure A in 57 % yield as a colorless oil: **^{1}H-NMR** ($CDCl_3$, 400 MHz): δ [ppm] = 7.91 (d, *J* = 8.3 Hz, 2H), 7.39 – 7.37 (m, 3H), 7.17 – 7.15 (m, 2H), 7.11 (d, *J* = 8.3 Hz, 2H), 6.10 (br. s, 1H), 4.50 (s, 2H), 3.90 (s, 3H), 3.50 (s, 2H), 3.31 (s, 9H). **^{13}C-NMR** ($CDCl_3$, 101 MHz): δ [ppm] = 171.1, 167.6, 166.9, 142.5, 140.2, 129.9, 129.7, 129.0, 128.7, 128.6, 127.9, 55.3, 52.1, 51.3,

40.9, 28.7 (3C). HRMS calculated for $C_{22}H_{27}N_2O_4$: 383.1971, found: 383.1962 ($[M+H]^+$), TLC (CH/EtOAc 1/1): R_f = 0.42.

*Methyl 4-(2-((2-(cyclohexylamino)-2-oxoethyl)(2-methylphenyl)amino)-2-oxoethyl)benzoate (**8e**).* Synthesized from **5**, cyclohexyl isocyanide (**7a**), paraformaldehyde (**4**), 2-methylaniline (**3b**) according to the general procedure A in 61 % yield as a colorless oil: **^{1}H-NMR** ($CDCl_3$, 400 MHz): δ [ppm] = 7.93 (d, *J* = 8.2 Hz, 2H), 7.39 – 7.32 (m, 3H), 7.23 (m, 1H), 7.10 (d, *J* = 8.1 Hz, 2H), 6.14 (d, *J* = 7.9 Hz, 1H), 4.58 (d, *J* = 14.5 Hz, 1H), 3.93 (s, 3H), 3.76 (d, *J* = 14.5 Hz, 1H), 3.78 (m, 1H), 2.11 (s, 3H), 1.92 – 1.82 (m, 2H), 1.75 – 1.60 (m, 2H), 1.45 – 1.25 (m, 3H), 1.20 – 1.10 (m, 3H). **^{13}C-NMR** ($CDCl_3$, 101 MHz): δ [ppm] = 171.6, 167.8, 167.0, 140.4, 140.0, 138.9, 130.7, 129.9, 129.2, 128.9, 127.7, 54.8, 52.3, 48.2, 40.9, 33.0, 25.6, 24.8, 21.4. HRMS calculated for $C_{25}H_{31}N_2O_4$: 423.2284, found: 423.2273 ($[M+H]^+$), TLC (CH/EtOAc 1/1): R_f = 0.30.

*Methyl 4-(2-((2-(cyclohexylamino)-2-oxoethyl)(3-methylphenyl)amino)-2-oxoethyl)benzoate (**8f**).* Synthesized from **5**, cyclohexyl isocyanide (**7a**), paraformaldehyde (**4**), 3-methylaniline (**3c**) according to the general procedure A in 75 % yield as a colorless oil: **^{1}H-NMR** ($CDCl_3$, 400 MHz): δ [ppm] = 7.94 (d, *J* = 8.2 Hz, 2H), 7.31 (s, 1H), 7.20 (d, 1H), 7.15 (d, *J* = 8.1 Hz, 2H), 6.97 (m, 2H), 6.18 (d, 1H), 5.32 (s, 1H), 4.25 (s, 2H), 3.93 (s, 3H), 3.59 (s, 2H), 2.34 (s, 3H), 1.90-1.82 (m, 2H), 1.70-1.64 (m, 2H), 1.42-1.25 (m, 3H), 1.23-1.06 (m, 3H). **^{13}C-NMR** ($CDCl_3$, 101 MHz): δ [ppm] = 171.6, 167.8, 167.0, 140.4, 140.0, 138.9, 130.7, 129.9, 129.2, 128.9, 127.7, 54.8, 52.3, 48.2, 40.9, 33.0, 25.6, 24.8, 21.2. HRMS calculated for $C_{25}H_{31}N_2O_4$: 423.2284, found: 423.2282 ($[M+H]^+$), TLC (CH/EtOAc 1/1): R_f = 0.30.

*Methyl 4-(2-((2-(cyclohexylamino)-2-oxoethyl)(4-methylphenyl)amino)-2-oxoethyl)benzoate (**8g**).* Synthesized from **5**, cyclohexyl isocyanide (**7a**), paraformaldehyde (**4**), 4-methylaniline 3d

according to the general procedure A in 58 % yield as a colorless oil: **^{1}H-NMR** ($CDCl_3$, 400 MHz): δ [ppm] = 7.92 (d, *J* = 8.3 Hz, 2H), 7.22-7.11 (m, 4H), 7.03 (d, *J* = 8.2 Hz, 2H), 6.16 (d, *J* = 8.0 Hz, 1H), 4.22 (s, 2H), 3.90 (s, 3H), 3.73 (m, 1H), 3.56 (s, 2H), 2.38 (s, 3H), 1.91-1.77 (m, 2H), 1.71-1.60 (m, 2H), 1.33 (m, 2H), 1.22-1.01 (m, 4H). **^{13}C-NMR** ($CDCl_3$, 101 MHz): *δ* [ppm] = 171.6, 167.8, 167.0, 140.4, 140.0, 138.9, 130.7, 129.9, 129.2, 128.9, 127.7, 54.8, 52.3, 48.2, 40.9, 33.0, 25.6, 24.8, 21.3. HRMS calculated for $C_{25}H_{31}N_2O_4$: 423.2284, found: 423.226 ($[M+H]^+$), TLC (CH/EtOAc 1/1): R_f = 0.30.

*Methyl 4-(2-((2-(cyclohexylamino)-2-oxoethyl)(2-ethylphenyl)amino)-2-oxoethyl)benzoate (**8h**).* Synthesized from **5**, cyclohexyl isocyanide (**7a**), paraformaldehyde (**4**), 2-ethylaniline (**3e**) according to the general procedure A in 54 % yield as a colorless oil: **^{1}H-NMR** ($CDCl_3$, 400 MHz): *δ* [ppm] = 7.91 (d, *J* = 8.3 Hz, 2H), 7.35 – 7.32 (m, 2H), 7.20 (m, 1H), 7.10 (m, 1H), 7.07 (d, *J* = 8.3 Hz, 2H), 6.43 (d, *J* = 8.3 Hz, 1H), 4.62 (d, *J* = 14.5 Hz, 1H), 3.90 (s, 3H), 3.68 (d, *J* = 14.5 Hz, 1H), 3.44 (s, 2H), 2.45 (ddt, *J* = 7.5 Hz, 2H), 1.90 – 1.79 (m, 2H), 1.69 – 1.61 (m, 2H), 1.40 – 1.25 (m, 3H), 1.19 (t, *J* = 7.6 Hz, 3H), 1.15 – 1.06 (m, 3H). **^{13}C-NMR** ($CDCl_3$, 101 MHz): *δ* [ppm] = 171.8, 167.5, 166.8, 140.8, 140.6, 139.8, 129.7 (2C), 129.6, 129.4, 129.2 (2C), 129.0, 128.8, 127.4, 54.5, 52.0, 48.0, 40.8, 32.9, 32.8, 25.5, 24.6, 23.4, 14.2. HRMS calculated for $C_{26}H_{32}N_2O_4Na$: 459.2260 found: 459.2268 ($[M+Na]^+$), TLC (CH/EtOAc 1/1): R_f = 0.29.

M*ethyl4-(2-((2-(cyclohexylamino)-2-oxoethyl)(3-(trifluoromethyl)phenyl)amino)-2-oxoethyl)-benzoate (**8i**).* Synthesized from **5**, cyclohexyl isocyanide (**7a**), paraformaldehyde (**4**), 2-trifluoro-aniline (**3f**) according to the general procedure A in 38 % yield as a colorless oil: **^{1}H-NMR** ($CDCl_3$, 400 MHz): *δ* [ppm] = 7.93 (d, *J*= 8.3 Hz, 2H), 7.80 (m, 1H), 7.56 (m, 3H), 7.27 (m, 1H), 7.15 (d, *J*= 8.2 Hz, 2H), 6.05 (d, *J*= 7.5 Hz, 1H), 4.85 (d, *J*= 15.1 Hz, 1H), 3.89 (s, 3H), 3.73 (m, 1H), 3.52 (d, *J*= 15.1 Hz, 1H), 3.46 (d, *J*= 15.4 Hz, 1H), 3.35 (d, *J*= 15.4 Hz, 1H), 1.85 (m, 2H) 1.65 (m, 2H)

1.58 (m, 1H) 1.30 (m, 2H) 1.16 (m, 3H). **^{19}F-NMR** ($CDCl_3$, 400 MHz): δ [ppm] = -66.99. **^{13}C-NMR** ($CDCl_3$, 75 MHz): δ [ppm] = 171.1, 167.2, 166.9, 140.1, 139.7, 133.7, 132.2, 129.7, 129.5, 129.2, 128.8, 127.6 (q, J = 5.2 Hz), 123.4 (q, J = 273.3 Hz), 54.2, 52.0, 48.3, 40.8, 32.9, 26.9, 25.4, 24.7. HRMS calculated for $C_{25}H_{28}F_3N_2O_4$: 477.2001, found: 477.1999 ($[M+H]^+$), TLC (CH/EtOAc 2/1): R_f = 0.30.

*Methyl 4-(2-((2-(cyclohexylamino)-2-oxoethyl)(phenyl)amino)-2-oxoethyl)-3-fluorobenzoate (**9a**)*. Synthesized from **6**, cyclohexyl isocyanide (**7a**), paraformaldehyde (**4**), aniline (**3**) according to the general procedure A in 87% yield as a yellowish solid: **^{1}H-NMR** ($CDCl_3$, 300 MHz): δ [ppm] = 7.76 (dd, J = 7.9, 1.6 Hz, 1H), 7.64 (dd, J = 10.3, 1.6 Hz, 1H), 7.42 (m, 2H), 7.37 (m, 1H), 7.28 (m, 2H), 7.25 (s, 1H), 6.20 (d, J = 8.6 Hz, 1H), 4.27 (s, 2H), 3.90 (s, 3H), 3.77 (m, 1H), 3.56 (s, 2H), 1.92 –1.85 (m, 2H), 1.72 – 1.65 (m, 2H), 1.62 – 1.56 (m, 1H), 1.38 – 1.30 (m, 2H), 1.20 – 1.10 (m, 3H). **^{13}C-NMR** ($CDCl_3$, 101 MHz): δ [ppm] = 170.4, 167.5, 165.8, 160.5 (d, J = 246.7 Hz), 142.4, 131.5 (d, J = 4.2 Hz), 131.0 (d, J = 7.8 Hz), 130.1 (2C), 128.7, 127.9 (d, J = 16.1 Hz), 127.7 (2C), 125.3 (d, J = 3.4 Hz), 116.2 (d, J = 24.0 Hz), 54.5, 52.3, 48.2, 34.8, 32.9, 25.5, 24.7. HRMS calculated for $C_{24}H_{28}FN_2O_4$: 427.2033, found: 427.2060 ($[M+H]^+$), TLC (CH/EtOAc 2/1): R_f = 0.30.

*Methyl 4-(2-((2-(cyclohexylamino)-2-oxoethyl)(2-methylphenyl)amino)-2-oxoethyl)-3-fluoro-benzoate (**9b**)*. Synthesized from **6**, cyclohexyl isocyanide (**7a**), paraformaldehyde (**4**), 2-methylaniline (**3b**) according to the general procedure A in 61% yield as a yellowish solid: **^{1}H-NMR** ($CDCl_3$, 300 MHz): δ [ppm] = 7.75 (dd, J = 7.9, 1.7 Hz, 1H), 7.64 (dd, J = 10.3, 1.6 Hz, 1H), 7.30 (dd, J = 8.3 Hz, 2H), 7.26 (m, 1H), 7.23 (m, 2H), 6.49 (d, J = 8.3 Hz, 1H), 4.56 (d, J = 14.6 Hz, 1H), 3.90 (s, 3H), 3,78 (J = 14.6 Hz, 1H), 3.77 (m, 1H), 3.42 (q, J = 16.1 Hz, 2H), 2.24 (s, 3H), 1.96 – 1.81 (m, 2H), 1.75 – 1.64 (m, 2H), 1.60-1.54 (m, 1H), 1.45-1.30 (m, 2H), 1.21 –

1.12 (m, 3H). **^{19}F-NMR** ($CDCl_3$, 400 MHz): δ [ppm] = -116.30. **^{13}C-NMR** ($CDCl_3$, 101 MHz): δ [ppm] = 170.7, 167.3, 165.9, 160.6 (d, *J* = 246.7 Hz), 141.0, 135.4, 131.8, 131.6 (d, *J* = 3.9 Hz), 131.1 (d, *J* = 7.6 Hz), 129.2, 128.6, 127.7, 127.6, 125.3 (d, *J* = 3.1 Hz), 116.3 (d, *J* = 23.9 Hz), 54.1, 52.2, 48.2, 34.6, 32.9 (2C), 25.5 (2C), 24.7, 17.4. HRMS calculated for $C_{25}H_{30}FN_2NaO_4$: 441.2190, found: 441.2203 ($[M+H]^+$), TLC (CH/EtOAc 2/1): R_f = 0.23.

*Methyl 4-(2-((2-(cyclohexylamino)-2-oxoethyl)(2-ethylphenyl)amino)-2-oxoethyl)-3-fluoro-benzoate (**9c**).* Synthesized from **6**, cyclohexyl isocyanide (**7a**), paraformaldehyde (**4**), 2-ethylaniline (**3e**) according to the general procedure A in 43% yield as a yellowish solid: **^{1}H-NMR** ($CDCl_3$, 300 MHz): δ [ppm] = 7.76 (d, *J*= 7.8 Hz, 1H), 7.65 (d, *J*= 10.2 Hz, 1H), 7.37 (d, *J*= 3.4 Hz, 2H), 7.27 (m, 1H), 7.23 (m, 2H), 6.48 (d, *J* = 7.8 Hz, 1H), 4.61 (d, *J* = 14.6 Hz, 1H), 3.91 (s, 3H), 3.78 (t, *J* = 14.7 Hz, 1H), 3.76 (d, *J*= 14.6 Hz, $1H_b$), 3.42 (dd, J_{H-F} = 50.2 Hz, J_{H-H} = 16.1 Hz, 2H), 2.58 (q, 2H, *J* = 7.4 Hz), 1.95-1.81 (m, 2H) 1.74-1.63 (m, 2H), 1.62-1.58 (m, 1H) 1.36 (m, 1H),1.29-1.22 (m, 3H), 1.25 (t, *J* = 7.6 Hz, 3H) 1.16 (m, 3H). **^{13}C-NMR** ($CDCl_3$,101 MHz): δ [ppm] = 170.9, 165.8, 160.6 (d, *J* = 246.9 Hz), 140.9, 140.5, 131.6 (d, *J* = 4.2 Hz), 131.1 (d, *J* = 7.8 Hz), 129.7, 129.4, 128.6, 127.7, 127.6, 125.3 (d, *J* = 3.4 Hz), 116.2 (d, *J* = 23.9 Hz), 54.6, 52.3, 48.1, 34.7, 32.9 (2C), 26.9, 25.5 (2C), 24.7, 23.3, 14.3. HRMS calculated for $C_{26}H_{32}FN_2O_4$: 455.2346, found: 455.2375 ($[M+H]^+$), TLC (CH/EtOAc 2/1): R_f = 0.19.

*Methyl 4-(2-((2-(cyclohexylamino)-2-oxoethyl)(2-trifluoromethylphenyl)amino)-2-oxoethyl)-3-fluorobenzoate (**9d**).* Synthesized from **6**, cyclohexyl isocyanide (**7a**), paraformaldehyde (**4**), 2-trifluoromethylaniline (**3f**) according to the general procedure A in 28% yield as a yellowish oil: **^{1}H-NMR** ($CDCl_3$, 300 MHz): δ [ppm] = 7.78 (m, 2H), 7.65 (m, 2H), 7.56 (m, 1H), 7.34 (m, 2H), 6.40 (s,1H), 4.82 (d, *J* = 15.0 Hz, 1H), 3.92 (s, 3H), 3.76 (m, 1H), 3.56 (d, J_{H-H} = 15.8 Hz, 1H),

3.42 (dd, $^{4}J_{H\text{-}F}$ = 49.2 Hz, $^{2}J_{H\text{-}H}$ = 16.3 Hz, 2H), 1,85 (m, 2H) 1.68 (m, 3H) 1.34 (m, 2H) 1.13 (m, 3H). **^{13}C-NMR** ($CDCl_3$, 101 MHz): δ [ppm] = 170.5, 167.3, 167.0 (d, *J* = 2.8 Hz), 160.6 (d, *J* = 247.0 Hz), 140.2 (d, *J* = 1.8 Hz), 134.0, 132.1, 131.8 (d, *J* = 4.0 Hz), 131.2 (d, *J* = 7.8 Hz), 129.7, 127.9 (q, *J* = 5.1 Hz), 127.5 (d, *J* = 16.1 Hz), 125.5 (d, *J* = 3.5 Hz), 123.4 (d, *J* = 273.1 Hz), 116.7 (q, *J* = 23.9 Hz), 116.3 (d, *J* = 24.0 Hz), 54.5, 52.5, 48.5, 33.0 (d, *J* = 5.3 Hz), 27.0, 25.6, 24.9 (d, *J* = 2.3 Hz). HRMS calculated for $C_{25}H_{27}F_4N_2O_4$: 495.1907, found: 495.1897 ($[M+H]^+$), TLC (CH/EtOAc 2/1): R_f = 0.08.

*General procedure B for the preparation of target compounds **1a-i** and **2a-d**.* The appropriate ester (1 equivalent) were dissolved 10 mL one-neck flask in 5 mL dichloromethane/methanol (1:2), cooled down to 0°C and treated with 20 equivalent hydroxylamine (50 wt% in water) dropwise and 10 equivalent powdered potassium hydroxide were added. The reaction mixture was stirred 15 min at 0 °C and additionally 2-4 h at room temperature and monitored via TLC. The solvent was removed under reduced pressure, the crude residue dissolved in 5 mL water and acidified with 1 N hydrochloric acid (pH: 8). The precipitated white solid was filtered, washed with water and dried at high vacuum. Additionally, the product was recrystallized or purified with prep-HPLC (ACN/H_2O+0.05% TFA-gradient).

*4-(2-((2-(Cyclohexylamino)-2-oxoethyl)(phenyl)amino)-2-oxoethyl)-N-hydroxybenzamide (**1a**).* Synthesized from **8a** according to the general procedure B in 45% yield as a white solid ^{1}**H-NMR** (DMSO-d_6, 400 MHz): δ [ppm] = 11.15 (br. s, 1H), 9.16 (br. s, 1H), 7.74 (d, *J* = 7.5 Hz), 7.62 (d, *J* = 7.8 Hz, 2H), 7.48 – 7.30 (m, 5H), 7.14 (d, *J* = 7.8 Hz, 2H), 4.18 (s, 2H), 3.57 – 3.39 (m, 3H), 1.75 – 1.58 (m, 4H), 1.58 – 1.46 (m, 1H), 1.31 – 1.16 (m, 2H), 1.13 – 1.01 (m, 3H). ^{13}**C-NMR** (DMSO-d_6, 101 MHz): δ [ppm] = 169.6, 166.6, 164.0, 143.0, 139.0, 130.8, 129.4 (2C), 129.2 (2C),

128.3 (2C), 127.9, 126.6 (2C), 52.0, 47,7, 40.0 (overlap DMSO), 32.4 (2C), 25.2, 24.5 (2C). HRMS calculated for $C_{23}H_{26}N_3O_4$: 408.1929, found: 408.1896 ($[M-H]^+$). HPLC purity: 97.1%.

4-(2-((2-(Benzyl)-2-oxoethyl)(phenyl)amino)-2-oxoethyl)-N-hydroxybenzamide ***(1b).*** Synthesized from **8b** according to the general procedure B in 70 % yield as a white solid: ^{1}**H-NMR** (DMSO-d_6, 400 MHz): δ [ppm] = 11.15 (br. s, 1H), 9.00 (br. s, 1H), 8.46 (t, *J* = 5.5 Hz, 1H); 7.63 (d, *J* = 8.0 Hz, 2H), 7.51 – 7.42 (m, 4H), 7.40 – 7.33 (m, 1H), 7.30 – 7.25 (m, 2H), 7.23 – 7.18 (m, 3H), 7.15 (d, *J* = 8.0 Hz, 2H), 4.30 (s, 2H), 4.28 (s, 2H), 3.50 (s, 2H). ^{13}**C-NMR** (DMSO-d_6, 101 MHz): δ [ppm] = 169.7, 167.8, 164.0, 142.9, 139.2, 139.0, 130.8, 129.5, 129.2 (2C), 128.3, 128.2 (4C), 128.0, 127.1 (2C), 126.7, 126.6 (2C), 52.3, 42.1, 40.2 (overlap DMSO). HRMS calculated for $C_{24}H_{23}N_3NaO_4$: 440.1586, found: 440.1580 ($[M+Na]^+$). HPLC purity: 95.3%.

4-(2-((2-(Butylamino)-2-oxoethyl)(phenyl)amino)-2-oxoethyl)-N-hydroxybenzamide ***(1c).*** Synthesized from **8c** according to the general procedure B in 45 % yield as a white solid: ^{1}**H-NMR** (DMSO-d_6, 400 MHz): δ [ppm] = 11.11 (br. s, 1H), 8.97 (br. s, 1H), 7.87 (t, *J* = 5.7 Hz, 1H), 7.62 (d, *J* = 8.0 Hz, 2H), 7.53 – 7.32 (m, 5H), 7.12 (d, *J* = 8.0 Hz, 2H), 4.20 (s, 2H), 3.47 (s, 2H), 3.04 (q, *J* = 6.5 Hz, 2H), 1.41 – 1.27 (m, 2H), 1.26 – 1.13 (m, 2H), 0,83 (t, *J* = 7.2 Hz, 3H). ^{13}**C-NMR** (DMSO-d_6, 101 MHz): δ [ppm] = 169.8, 167.5, 164.1, 143.0, 138.9, 131.0, 129.5 (2C), 129.2 (2C), 128.9, 128.7, 128.3 (2C), 128.0, 126.6, 52.2, 40.0 (overlap DMSO) 31.2, 19.5, 13.7. HRMS calculated for $C_{21}H_{25}N_3NaO_4$: 406.1743, found: 432.1735 ($[M+Na]^+$). HPLC purity: 95.8%.

4-(2-((2-(tert-Butylamino)-2-oxoethyl)(phenyl)amino)-2-oxoethyl)-N-hydroxybenzamide ***(1d).*** Synthesized from **8d** according to the general procedure B in 41 % yield as a white solid: ^{1}**H-NMR** (DMSO-d_6, 400 MHz): δ [ppm] = 10.97 (br. s, 1H), 9.06 (br. s, 1H), 7.63 (d, *J* = 7.9 Hz, 2H), 7.50 – 7.31 (m, 6H), 7.14 (d, *J* = 7.9 Hz, 2H), 4.15 (s, 2H), 3.46 (s, 2H), 1.24 (s, 9H). ^{13}**C-NMR**

(DMSO-d_6, 101 MHz): δ [ppm] = 169.5, 166.9, 164.0, 143.0, 139.0, 130.9, 129.4 (2C), 129.2 (2C), 128.3 (2C), 127.9, 126.6 (2C), 52.3, 50.2, 40.0 (overlap with DMSO), 28.5 (3C). HRMS calculated for $C_{21}H_{25}N_3NaO_4$: 406.1743, found: 406.1736 ($[M+Na]^+$). HPLC purity: 98.1%.

*4-(2-((2-(Cyclohexylamino)-2-oxoethyl)(2-methylphenyl)amino)-2-oxoethyl)-N-hydroxy-benzamide (**1e**).* Synthesized from **8e** according to the general procedure B in 80 % yield as a white solid: ^{1}**H-NMR** (DMSO-d_6, 400 MHz): δ [ppm] = 11.06 (br. s, 1H), 9.00 (br. s, 1H), 7.69 (d, *J* = 7.7 Hz, 1H), 7.61 (d, *J* = 8.2 Hz, 2H), 7.45 – 7.39 (m, 1H), 7.37 – 7.30 (m, 2H), 7.29 – 7.22 (m, 1H), 7.08 (d, *J* = 8.2 Hz, 2H), 4.62 (d, *J* = 15.7 Hz, 1H), 3.54 (d, *J* = 15.7 Hz, 1H), 3.54 – 3.44 (m, 1H), 3.37 (d, *J* = 15.3 Hz, 1H), 3.30 (d, *J* = 15.3 Hz, 1H, overlap with water), 2.11 (s, 3H), 1.77 – 1.56 (m, 4H), 1.56 – 1.46 (m, 1H), 1.31 – 1.19 (m, 2H), 1.18 – 0.98 (m, 3H). ^{13}**C-NMR** (DMSO-d_6, 101 MHz): δ [ppm] = 169.7, 166.4, 164.0, 141.4, 138.7, 135.5, 131.2, 130.9, 129.6, 129.1 (2C), 128.5, 127.0, 126.6 (2C), 50.8, 47.6, 40.0 (overlap with DMSO), 32.4, 32.3, 25.2, 24.5 (2C), 17.2. HRMS calculated for $C_{24}H_{29}N_3NaO_4$: 446.2056, found: 446.2049 ($[M+Na]^+$). HPLC purity: 95.5%.

*4-(2-((2-(Cyclohexylamino)-2-oxoethyl)(3-methylphenyl)amino)-2-oxoethyl)-N-hydroxybenzamide (**1f**).* Synthesized from **8f** according to the general procedure B in 59 % yield as a white solid: ^{1}**H-NMR** (DMSO-d_6, 400 MHz): δ [ppm] = 11.12 (br. s, 1H), 9.21 (br. s, 1H), 7.74 (d, *J* = 7.3 Hz, 1H), 7.63 (d, *J* = 7.9 Hz, 2H), 7.31 (t, *J* = 7.6 Hz, 1H), 7.18 (m, 3H), 7.12 (d, *J* = 7.9 Hz, 2H), 4.61 (s, 2H), 3.48 (m, 1H), 3.46 (s, 2H), 2.29 (s, 3H), 1.72 – 1.57 (m, 4H), 1.50 – 1.48 (m, 1H), 1.28 – 1.17 (m, 2H), 1.16 – 1.02 (m, 3H). ^{13}**C-NMR** (DMSO-d_6, 101 MHz): δ [ppm] = 169.6, 166.6, 164.0, 142.9, 138.9, 138.7, 131.3, 129.2, 129.1 (2C), 128.8, 128.5, 126.5 (2C), 125.2, 52.0, 47.7, 39.9 (overlap with DMSO), 32.4 (2C), 25.2, 24.5 (2C), 20.8. HRMS calculated for $C_{24}H_{29}N_3NaO_4$: 446.2056, found: 446.2055 ($[M+Na]^+$). HPLC purity: 95.5%.

*4-(2-((2-(Cyclohexylamino)-2-oxoethyl)(3-methylphenyl)amino)-2-oxoethyl)-N-hydroxybenzamide (**1g**).* Synthesized from **8g** according to the general procedure B in 39 % yield as a white solid: ^{1}**H-NMR** (DMSO-d_6, 400 MHz): δ [ppm] = 11.13 (br. s., 1H), 8.97 (br. s., 1H), 7.72 (d, *J* = 7.2 Hz, 1H), 7.62 (d, *J* = 7.7 Hz, 2H), 7.27-7.24 (d, *J* = 7.9 Hz, 2H), 7.15-7.13 (d, *J* = 7.7 Hz, 2H), 4.15 (s, 2H), 3.39 (m, 1H), 2.32 (s, 3H), 1.70 - 1.62 (m, 3H), 1.52 - 1.48 (m, 2H), 1.28 - 1.18 (m, 3H), 1.16 - 1.04 (m, 2H). ^{13}**C-NMR** (DMSO-d_6, 101 MHz): δ [ppm] = 169.6, 166.5, 140.4, 139.1, 137.3, 136.6, 130.8, 129.9 (2C), 129.2 (2C), 128.0 (2C), 126.6 (2C), 52.0, 47.6, 39.9 (overlaped with DMSO), 32.4 (2C), 25.2, 24.5 (2C), 20.6. HRMS calculated for $C_{24}H_{29}N_3NaO_4$: 446.2056, found: 446.2050 ($[M+Na]^+$). HPLC purity: 95.4%.

*4-(2-((2-(Cyclohexylamino)-2-oxoethyl)(2-ethylphenyl)amino)-2-oxoethyl)-N-hydroxy-benzamide (**1h**).* Synthesized from **8h** according to the general procedure B in 49% yield as a white solid: **^{1}H-NMR** (DMSO-d_6, 400 MHz): δ [ppm] = 11.34 (br. s., 1H), 8.98 (br. s., 1H), 7.90 (d, *J* = 7.9 Hz, 1H), 7.61 (d, *J* = 8.2 Hz, 1H), 7.44 (m, 1H), 7.36 (m, 2H), 7.25 (m, 1H), 7.07 (d, *J* = 8.2 Hz, 2H), 4.64 (d, *J* = 15.8 Hz, 1H), 3.51 (d, *J* = 15.8 Hz, 1H), 3,48 (m, 1H), 3.33 (q, *J* = 7.7 Hz, 2H), 3.30 (s, 2H), 1.73 – 1.57 (m, 4H), 1.56 – 1.42 (m, 1H), 1.31 – 1.18 (m, 2H), 1.14 (t, *J* = 7.7 Hz, 3H), 1.10 – 1.01 (m, 2H). **^{13}C-NMR** (DMSO-d_6, 101 MHz): δ [ppm] = 169.8, 166.3, 163.9, 140.9, 140.8, 138.3, 131.4, 129.5, 129.3, 129.2, 129.0 (2C), 128.7, 126.8, 126.5 (2C), 51.5, 47.6, 32.4, 32.3, 25.1, 24.5, 24.4, 22.9, 14.1. HRMS calculated for $C_{25}H_{31}N_3NaO_4$: 460.2212, found: 460.2209. ($[M+Na]^+$). HPLC purity: 95.4%.

*4-(2-((2-(Cyclohexylamino)-2-oxoethyl)(2-trifluormethylphenyl)amino)-2-oxoethyl)-N-hydroxy-benzamide (**1i**).* Synthesized from **8i** according to the general procedure B in 34% yield as a white

solid: **^{1}H-NMR** (methanol-d_4, 400 MHz): δ [ppm] = 10.0 (br. s., 1H), 7.88 (d, *J* = 7.3, 1H), 7.79 (d, *J* = 7.6 Hz, 1H), 7.72 – 7.68 (m, 1H), 7.65 (d, *J* = 8.1 Hz, 3H), 7.18 (d, *J* = 8.1 Hz, 2H), 4.85 (d, *J* = 16.3 Hz, 1H), 3.68 – 3.59 (m, 1H), 3.60 (d, *J* = 16.1, 1H), 3.52 – 3.37 (m, 2H), 1.93 – 1.56 (m, 5H), 1.38 – 1.30 (m, 2H), 1.23 – 1.12 (m, 3H). **^{13}C-NMR** (methanol-d_4, 101 MHz): δ [ppm] = 173.1, 168.9, 167.6, 141.6, 139.5 (d, *J* = 4.6 Hz), 135.1, 133.4, 132.7, 131.0, 130.6 (2C), 128.7 (q, *J* = 5.1 Hz), 128.4 (q, *J* = 29.7 Hz), 127.9 (2C), 124.9 (q, *J* = 272.5 Hz), 54.0, 49.9, 41.6, 33.7, 33.7, 26.6, 26.0 (2C). HRMS calculated for $C_{24}H_{26}F_3N_3NaO_4$: 500.1750, found: 500.1750 ($[M+Na]^+$). HPLC purity: 98.5%.

*4-(2-((2-(Cyclohexylamino)-2-oxoethyl)(phenyl)amino)-2-oxoethyl)-3-fluoro-N-hydroxy-benzamide (**2a**).* Synthesized from **9a** according to the general procedure B in 71% yield as a white solid: **^{1}H-NMR** (DMSO-d_6, 400 MHz): δ [ppm] =10.01 (br. s, 1H), 7.74 (d, *J* = 7.8 Hz, 1H), 7.50 (d, *J* = 7.9 Hz, 1H), 7.44 (d, *J* = 4.5 Hz, 4H), 7.33 (t, *J* = 7.8 Hz, 2H), 4.19 (s, 1H), 3.58 – 3.23 (m, 4H), 1.74 – 1.59 (m, 4H), 1.52 (dt, *J* = 13.1, 3.8 Hz, 1H), 1.21 (tt, *J* = 10.7, 3.0 Hz, 2H), 1.16 – 1.04 (m, 3H). **^{13}C-NMR** (DMSO-d_6, 101 MHz): δ [ppm] =168.7, 166.5, 162.7, 160.1 (d, *J* = 244.6 Hz), 142.8, 133.8 (d, *J* = 6.8 Hz), 131.9, 129.6 (2C), 128.2 (2C), 128.1, 125.9 (d, *J* = 16.1 Hz), 122.4, 113.1 (d, *J* = 23.6 Hz), 64.9, 52.1, 47.7, 33.7, 32.4, 25.2, 24.5, 15.2. HRMS calculated for $C_{23}H_{26}FN_3NaO_4$, 450.1805, found: 450.1795 ($[M+Na]^+$). HPLC purity: 95.4%.

*4-(2-((2-(Cyclohexylamino)-2-oxoethyl)(2-methylphenyl)amino)-2-oxoethyl)-3-fluoro-N-hydroxy-benzamide (**2b**).* Synthesized from **9b** according to the general procedure B in 44% yield as a white solid: **^{1}H-NMR** (DMSO-d_6, 400 MHz): δ = 7.70 (d, *J* = 7.8 Hz, 1H), 7.48 (ddd, *J* = 10.1, 7.9, 1.7 Hz, 2H), 7.42 (dd, *J* = 10.7, 1.6 Hz, 1H), 7.38 – 7.26 (m, 3H), 4.61 (d, *J* = 15.7 Hz, 1H), 3.57 (d, *J* = 15.7 Hz, 1H), 3.50 (dq, *J* = 7.1, 3.4 Hz, 1H), 3.41 – 3.34 (m, 2H), 2.22 (s, 3H), 1.77 – 1.57 (m, 5H), 1.21 (dddd, *J* = 19.9, 14.3, 6.7, 2.7 Hz, 3H), 1.14 – 1.03 (m, 2H). **^{13}C NMR**

(DMSO-d_6, 101 MHz): δ [ppm] = 168.7, 166.3, 162.6, 160.1 (d, J = 244.8 Hz), 141.2, 135.5, 133.9 (d, J = 7.3 Hz), 132.0, 131.2, 129.5, 128.5, 127.0, 125.6 (d, J = 16.2 Hz), 122.3, 113.0 (d, J = 23.4 Hz), 50.9, 47.6, 33.6, 32.4, 32.3, 25.2, 24.5, 24.4, 17.0. HRMS calculated for $C_{24}H_{28}FN_3NaO_4$: 464,1962, found: 464.1964 ($[M+Na]^+$). HPLC purity (250 nm): 95.6%.

*4-(2-((2-(Cyclohexylamino)-2-oxoethyl)(2-ethylphenyl)amino)-2-oxoethyl)-3-fluoro-N-hydroxy-benzamide (**2c**).* Synthesized from **9c** according to the general procedure B in 61% yield as a white solid: **^{1}H-NMR** (methanol-d_4, 400 MHz): δ [ppm] = 7.81 (weak d, 1H), 7.57 (d, J = 7.6 Hz, 1H), 7.34 (d, J = 7.8 Hz, 2H), 7.29 – 7.20 (m, 2H), 7.23 – 7.06 (m, 2H), 4.50 (d, J = 15.7 Hz, 1H), 3.80 - 2.90 (m, 4H, H_2O peak), 2.49 – 2.37 (m, 2H), 1.70 – 1.43 (m, 4H), 1.37 (d, J = 11.4 Hz, 1H), 1.08 (s, 2H), 1.04 (t, J = 7.5 Hz, 3H), 0.93 (dq, J = 22.6, 10.6, 9.3 Hz, 3H). **^{13}C-NMR** (methanol-d_4, 101 MHz): δ [ppm] = 178.6, 175.9, 172.2, 169.7 (d, J = 244.4 Hz), 150.5, 150.26, 144.4 (d, J = 5.6 Hz), 139.1, 138.9, 138.4, 136.5, 134.4 (d, J = 15.4 Hz), 131.7, 122.4 (d, J = 23.4 Hz), 61.2, 57.2, 43.2, 41.9 (2C), 34.7, 34.0 (2C), 32.3, 23.7. HRMS calculated for $C_{25}H_{30}FN_3NaO_4$: 478,2118, found: 478.2122 ($[M+Na]^+$). HPLC purity: 97.0%.

*4-(2-((2-(Cyclohexylamino)-2-oxoethyl)(2-trifluoromethylphenyl)amino)-2-oxoethyl)-3-fluoro-N-hydroxy-benzamide (**2d**).* Synthesized from **9d** according to the general procedure B in 34% yield as a white solid: **^{1}H-NMR** (methanol-d_4, 400 MHz): δ [ppm] = 7.88 (t, J = 6.9 Hz, 2H), 7.74 (t, J = 7.3 Hz, 1H), 7.66 (t, J = 7.6 Hz, 1H), 7.51 (dd, J = 7.9, 1.5 Hz, 1H), 7.43 – 7.35 (m, 2H), 4.84 (d, J = 16.3 Hz, 1H), 3.62 (d, J = 15.9 Hz, 2H), 3.55 – 3.33 (m, 2H), 1.92 – 1.55 (m, 5H), 1.35 (qdd, J = 13.2, 5.8, 3.1 Hz, 2H), 1.26 – 1.07 (m, 3H). **^{13}C-NMR** (methanol-d_4, 101 MHz): δ [ppm] = 172.0, 168.9, 166.4, 162.1 (d, J = 246.4 Hz), 141.5 (d, J = 10.4 Hz), 135.2, 134.9 (d, J = 7.3 Hz), 133.4, 133.1 (d, J = 3.9 Hz), 131.0, 129.2 – 128.6 (2C), 126.9 (d, J = 16.1 Hz), 124.9 (q, J = 265.3 Hz), 123.6 (d, J = 3.2 Hz), 114.7 (d, J = 24.2 Hz), 54.1, 49.9, 35.1, 33.7. 33.6, 26.6, 26.0 (2C).

HRMS calculated for $C_{24}H_{25}F_4N_3NaO_4$: 518.1679, found: 518.1663 ($[M+Na]^+$). HPLC purity: 99.9%.

4.2. Molecular docking

For the molecular docking the available protein structure of human HDAC6 was downloaded from the Protein Data Bank (PDB; PDB ID: 5EDU).[20] Only chain A was used for the docking. The protein was prepared using the software Molecular Operating Environment (MOE, Chemical Computing Group, version 2022.02)[31] by adding hydrogen atoms and building missing loops. Additionally, water molecules and ions (except the catalytic zinc ion) were removed from the crystal structure. The active water molecule (H_2O 921) from the crystal structure of *Danio rerio* HDAC6 (PDB ID: 5EF7)[20] was placed to the active site by structural alignment of both protein structures. Compound **2b** was drawn with ChemDraw (version 21.0.0.28) in its deprotonated form and prepared in MOE by generating the 3D structure and energy minimization using AMBER:EHT force field. The docking experiment was performed with GOLD[32] in combination with the HERMES visualizer (Cambridge Crystallographic Data Centre, version 2022.3.0). The active site was defined by the co-crystallized ligand within a radius of 15 Å. All poses were optimized within 50 GA runs and scored with ChemPLP. The early termination option of the docking runs was not allowed. The search efficacy was set to 200%. The docking was carried out with a scaffold match constraint to place the ligand onto a given scaffold location within the active site. The hydroxamate substructure (CONO) of the co-crystallized ligand in *Danio rerio* HDAC6 (PDB ID: 5EF7) was used as a template. The docking solutions were visual inspected according to a proper coordination of the zinc ion and a reasonable orientation of the cap groups. The pose depicted in Figure 3 represents the second top ranked docking solution out of 50.

4.3. Biological evaluation

4.3.1. Inhibition assay for HDAC1, 2, 3, and 6.

The *in vitro* inhibitory activities against HDAC1–3 and HDAC6 were measured using a previously published protocol.[33] For test compounds and controls, serial dilutions of the respective DMSO-stock solution in assay buffer (50 mM Tris−HCl, pH 8.0, 137 mM NaCl, 2.7 mM KCl, 1.0 mM $MgCl_2$•6 H_2O, 0.1 mg/mL BSA), were prepared and 5.0 µL of this serial dilution were transferred into OptiPlate-96 black micro-plates (PerkinElmer). 35 µL of the fluorogenic substrate ZMAL (Z-Lys(Ac)-AMC)[34] (21.43 µM in assay buffer) and 10 µL enzyme solution (human recombinant HDAC1 (BPS Bioscience, Catalog# 50051); HDAC2 (BPS Bioscience, Catalog# 50052); HDAC3/NcoR2 (BPS Bioscience, Catalog# 50003); HDAC6 (BPS Bioscience, Catalog# 50006). The total assay volume of 50 µL (max. 1% DMSO) was incubated at 37 °C for 90 min. Subsequently, 50 µL trypsin solution (0.4 mg/mL trypsin in buffer: 50 mM Tris−HCl, pH 8.0, 100 mM NaCl) was added, followed by additional 30 min of incubation at 37 °C. Fluorescence (excitation: 355 nm, emission: 460 nm) was measured using an Ascent Fluoroskan microplate reader (Thermo Scientific). All compounds were evaluated in duplicates in at least two independent experiments.

4.3.2. Cell culture

Leukemia cell lines were provided from the German collection of microorganisms and cell culture (DSMZ, Braunschweig, Germany) and two healthy fibroblast control cells (ATCC, Manassas, VA) were cultured according to the supplier's recommendations. All cell lines were cultured in RPMI1640 with 10-20% fetal bovine serum at 37°C with 5% CO_2. In general cells were only used for experiments if the viability exceeded 90%.

4.3.3. High throughput drug screening

Compounds were dissolved in DMSO as 10 mM stock solutions.[12] Plates for drug screening were preprinted via the Tecan D300e in a 384 well set up and stored afterward at -80 °C. All plates were individually randomized to avoid plate effects, and at least one row/column of the outer wells was used as an evaporation guard. Wells with lower DMSO content were normalized to the well with the highest DMSO volume. The cell viability and density were determined prior to the seeding via the Vi-CELL BLU cell counter. Cell lines were seeded in fresh media at 0.04 x 10^6 cell/mL density with the help of a Multidrop reagent dispenser. After 72 hours CellTiter-Glo reagent was added and the luminescence was determined by a Tecan Spark microplate reader. The initial determination of the experimental inhibitors used seven different compound doses ranging from 0.005 µM to 25 µM. All three cell lines were measured in biological triplicates. The focused screening was measured in technical triplicates and with 12 different concentrations from 0.005 µM to 25 µM. The viability [%] was determined by using the mean of the DMSO wells as a reference. Drug response curves & IC_{50} values were determined via prism software (GraphPad Prism Inc., San Diego, CA) using (log(inhibitor) vs. normalized response – Variable slope) function. Heatmaps were generated with the help of the R package complex heatmap.

4.3.4. Combinatorial drug screening

A matrix drug screening approach was utilized to investigate drug synergy..[12] Both **1g** and **2b** were combined with decitabine with an increased concentration in an 8 x 8 dose-response matrices (**1g**: 0.05 - 4 µM, **2b**: 0.05 – 4 µM, Decitabine 0.025 – 10 µM). Viability was assessed after a 72-hour

period employing the CellTiter-Glo luminescent assay, as detailed earlier (Spark, Tecan). The ZIP scores and graphical analysis were calculated with the help of the R SynergyFinder package.

4.3.5. Immunoblotting

Cells were treated with the indicated concentration of compound over the course of 24 hours in cell culture dishes. 0.5 x 10^6 cells/mL were seeded in 10 mL of media. Cells were washed three times with cold PBS and snap-frozen in liquid nitrogen. Lysis was accomplished via Pierce RIPA buffer (with cOmplete Protease Inhibitor cocktail, PhosSTOP & Dithiothreitol). After the removal of DNA the protein concentration was determined using a Pierce BCA protein assay kit (Thermo Fisher Scientific,Waltham, MA). All samples were mixed with 5x laemmli sample buffer and heated at 95°C for 5 minutes to ensure protein denaturation. 20 µg of protein were loaded on an SDS polyacrylamide gel. Afterward, the proteins were transferred from the gel to a nitrocellulose membrane in 1x tris-glycine transfer buffer with 10% methanol at 100 mV for 90 minutes.

3% bovine serum albumin (BSA) in tris buffered saline with Tween (TBST) was used for one hour to block the membrane and prevent unspecific antibody binding. Membranes were incubated with BSA diluted antibody solutions (1:1000) overnight at 4 °C. Antibodies used were anti-acetyl-α-tubulin (catalog no. 5335), anti-acetyl-histone H3 (catalog no. 9677S), and anti-β-actin (catalog no. 5125S) or anti-GAPDH (catalog no. 97166), following the supplier's guidelines (Cell Signaling Technology, Danvers, MA). The next day the membranes were washed three times with TBST. Horsereddish peroxidase (HRP) coupled secondary antibodies (Cell Signaling Technology) were diluted 1:1000 in a BSA solution and the membranes were incubated for 2 hours. Blots were visualized using Simple Western Jess machine (Biotechne).

4.3.5. Annexin PI staining

Leukemia cells (0.1 x 10^6 cells/mL) were seeded in 1 mL in 24 well plates and treated for 48 hours at the indicated concentrations. The treated cells were washed once with PBS and afterward treated with Annexin-PI-staining solution for 15 minutes at 4°C, following the supplier's guidelines (Invitrogen, Carlsbad, CA). FACS analysis was done via the Beckman Coulter CytoFLEX. Significance was calculated via an unpaired t-test.

Supplementary Data

Supplementary data (^{1}H- and ^{13}C-NMR spectra, HPLC chromatograms) related to this article can be found online.

Funding Sources

This work was funded in part by the Deutsche Forschungsgemeinschaft (DFG, German Research Foundation) 270650915 (Research Training Group GRK 2158, TP 2d) and BH 162/4-1 (528968169) to S.B. S.B. additionally acknowledges the financial support from Elterninitiative Kinderkrebsklinik e.V. A.B. acknowledges the financial support from Katharina-Hardt Foundation, Christiane und Claudia Hempel foundation and Löwenstern e.V.

References

(1) Biel, M.; Wascholowski, V.; Giannis, A. Epigenetics - An Epicenter of Gene Regulation: Histones and Histone-Modifying Enzymes. *Angew. Chem. Int. Ed.* **2005**, *44* (21), 3186–3216. https://doi.org/10.1002/anie.200461346.

(2) Mottamal, M.; Zheng, S.; Huang, T.; Wang, G. Histone Deacetylase Inhibitors in Clinical Studies as Templates for New Anticancer Agents. *Molecules* **2015**, *20* (3), 3898–3941. https://doi.org/10.3390/molecules20033898.

(3) Witt, O.; Deubzer, H. E.; Milde, T.; Oehme, I. HDAC Family: What Are the Cancer Relevant Targets? *Cancer Lett.* **2009**, *277* (1), 8–21. https://doi.org/10.1016/j.canlet.2008.08.016.

(4) Jenke, R.; Reßing, N.; Hansen, F. K.; Aigner, A.; Büch, T. Anticancer Therapy with HDAC Inhibitors: Mechanism-Based Combination Strategies and Future Perspectives. *Cancers* **2021**, *13* (4), 634. https://doi.org/10.3390/cancers13040634.

(5) West, A. C.; Johnstone, R. W. New and Emerging HDAC Inhibitors for Cancer Treatment. *J Clin Invest.* **2014**, *124* (1), 30–39. https://doi.org/10.1172/JCI69738.30.

(6) Sinatra, L.; Vogelmann, A.; Friedrich, F.; Tararina, M. A.; Neuwirt, E.; Colcerasa, A.; König, P.; Toy, L.; Yesiloglu, T. Z.; Hilscher, S.; Gaitzsch, L.; Papenkordt, N.; Zhai, S.; Zhang, L.; Romier, C.; Einsle, O.; Sippl, W.; Schutkowski, M.; Gross, O.; Bendas, G.; Christianson, D. W.; Hansen, F. K.; Jung, M.; Schiedel, M. Development of First-in-Class Dual Sirt2/HDAC6 Inhibitors as Molecular Tools for Dual Inhibition of Tubulin Deacetylation. *J. Med. Chem.* **2023**, *66* (21), 14787–14814.

https://doi.org/10.1021/acs.jmedchem.3c01385.

(7) Ho, T. C. S.; Chan, A. H. Y.; Ganesan, A. Thirty Years of HDAC Inhibitors: 2020 Insight and Hindsight. *J. Med. Chem.* **2020**, *63* (21), 12460–12484. https://doi.org/10.1021/acs.jmedchem.0c00830.

(8) Roche, J.; Bertrand, P. Inside HDACs with More Selective HDAC Inhibitors. *Eur. J. Med. Chem.* **2016**, *121*, 451–483. https://doi.org/10.1021/jm400179b.

(9) Bertrand, P. Inside HDAC with HDAC Inhibitors. *Eur. J. Med. Chem.* **2010**, *45* (6), 2095–2116. https://doi.org/10.1016/j.ejmech.2010.02.030.

(10) Melesina, J.; Simoben, C. V.; Praetorius, L.; Bülbül, E. F.; Robaa, D.; Sippl, W. Strategies To Design Selective Histone Deacetylase Inhibitors. *ChemMedChem* **2021**, *16* (9), 1336–1359. https://doi.org/10.1002/cmdc.202000934.

(11) Krieger, V.; Hamacher, A.; Cao, F.; Stenzel, K.; Gertzen, C. G. W.; Schäker-Hübner, L.; Kurz, T.; Gohlke, H.; Dekker, F. J.; Kassack, M. U.; Hansen, F. K. Synthesis of Peptoid-Based Class I-Selective Histone Deacetylase Inhibitors with Chemosensitizing Properties. *J. Med. Chem.* **2019**, *62* (24), 11260–11279. https://doi.org/10.1021/acs.jmedchem.9b01489.

(12) Reßing, N.; Schliehe-Diecks, J.; Watson, P. R.; Sönnichsen, M.; Cragin, A. D.; Schöler, A.; Yang, J.; Schäker-Hübner, L.; Borkhardt, A.; Christianson, D. W.; Bhatia, S.; Hansen, F. K. Development of Fluorinated Peptoid-Based Histone Deacetylase (HDAC) Inhibitors for Therapy-Resistant Acute Leukemia. *J. Med. Chem.* **2022**, *65* (22), 15457–15472. https://doi.org/10.1021/acs.jmedchem.2c01418.

(13) König, B.; Watson, P. R.; Reßing, N.; Cragin, A. D.; Schäker-Hübner, L.; Christianson, D. W.; Hansen, F. K. Difluoromethyl-1,3,4-Oxadiazoles Are Selective, Mechanism-Based, and Essentially Irreversible Inhibitors of Histone Deacetylase 6. *J. Med. Chem.* **2023**, *66* (19), 13821–13837. https://doi.org/10.1021/acs.jmedchem.3c01345.

(14) Depetter, Y.; Geurs, S.; De Vreese, R.; Goethals, S.; Vandoorn, E.; Laevens, A.; Steenbrugge, J.; Meyer, E.; de Tullio, P.; Bracke, M.; D'hooghe, M.; De Wever, O. Selective Pharmacological Inhibitors of HDAC6 Reveal Biochemical Activity but Functional Tolerance in Cancer Models. *Int. J. Cancer* **2019**, *145* (3), 735–747. https://doi.org/10.1002/ijc.32169.

(15) Reßing, N.; Sönnichsen, M.; Osko, J. D.; Schöler, A.; Schliehe-Diecks, J.; Skerhut, A.; Borkhardt, A.; Hauer, J.; Kassack, M. U.; Christianson, D. W.; Bhatia, S.; Hansen, F. K. Multicomponent Synthesis, Binding Mode, and Structure–Activity Relationship of Selective Histone Deacetylase 6 (HDAC6) Inhibitors with Bifurcated Capping Groups. *J. Med. Chem.* **2020**, *63* (18), 10339–10351. https://doi.org/10.1021/acs.jmedchem.9b01888.

(16) Mackwitz, M. K. W.; Hamacher, A.; Osko, J. D.; Held, J.; Schöler, A.; Christianson, D. W.; Kassack, M. U.; Hansen, F. K. Multicomponent Synthesis and Binding Mode of Imidazo[1,2-a]Pyridine-Capped Selective HDAC6 Inhibitors. *Org. Lett.* **2018**, *20* (11), 3255–3258. https://doi.org/10.1021/acs.orglett.8b01118.

(17) Pflieger, M.; Sönnichsen, M.; Horstick-Muche, N.; Yang, J.; Schliehe-Diecks, J.; Schöler, A.; Borkhardt, A.; Hamacher, A.; Kassack, M. U.; Hansen, F. K.; Bhatia, S.; Kurz, T. Oxa Analogues of Nexturastat A Demonstrate Improved HDAC6 Selectivity and Superior Antileukaemia Activity. *ChemMedChem* **2021**, *16* (11), 1799–1804.

https://doi.org/10.1002/cmdc.202001011.

(18) Reßing, N.; Marquardt, V.; Gertzen, C. G. W.; Schöler, A.; Schramm, A.; Kurz, T.; Gohlke, H.; Aigner, A.; Remke, M.; Hansen, F. K. Design, Synthesis and Biological Evaluation of β-Peptoid-Capped HDAC Inhibitors with Anti-Neuroblastoma and Anti-Glioblastoma Activity. *MedChemComm* **2019**, *10* (7), 1109–1115. https://doi.org/10.1039/c8md00454d.

(19) Miyake, Y.; Keusch, J. J.; Wang, L.; Saito, M.; Hess, D.; Wang, X.; Melancon, B. J.; Helquist, P.; Gut, H.; Matthias, P. Structural Insights into HDAC6 Tubulin Deacetylation and Its Selective Inhibition. *Nat. Chem. Biol.* **2016**, *12* (9), 748–754. https://doi.org/10.1038/nchembio.2140.

(20) Hai, Y.; Christianson, D. W. Histone Deacetylase 6 Structure and Molecular Basis of Catalysis and Inhibition. *Nat. Chem. Biol.* **2016**, *12* (9), 741–747. https://doi.org/10.1038/nchembio.2134.

(21) Sinatra, L.; Yang, J.; Schliehe-Diecks, J.; Dienstbier, N.; Vogt, M.; Gebing, P.; Bachmann, L. M.; Sönnichsen, M.; Lenz, T.; Stühler, K.; Schöler, A.; Borkhardt, A.; Bhatia, S.; Hansen, F. K. Solid-Phase Synthesis of Cereblon-Recruiting Selective Histone Deacetylase 6 Degraders (HDAC6 PROTACs) with Antileukemic Activity. *J. Med. Chem.* **2022**, *65* (24), 16860–16878. https://doi.org/10.1021/acs.jmedchem.2c01659.

(22) Shen, S.; Benoy, V.; Bergman, J. A.; Kalin, J. H.; Frojuello, M.; Vistoli, G.; Haeck, W.; Van Den Bosch, L.; Kozikowski, A. P. Bicyclic-Capped Histone Deacetylase 6 Inhibitors with Improved Activity in a Model of Axonal Charcot–Marie–Tooth Disease. *ACS Chem. Neurosci.* **2016**, *7* (2), 240–258. https://doi.org/10.1021/acschemneuro.5b00286.

(23) Sandrone, G.; Cukier, C. D.; Zrubek, K.; Marchini, M.; Vergani, B.; Caprini, G.; Fossati, G.; Steinkühler, C.; Stevenazzi, A. Role of Fluorination in the Histone Deacetylase 6 (HDAC6) Selectivity of Benzohydroxamate-Based Inhibitors. *ACS Med. Chem. Lett.* **2021**, *12* (11), 1810–1817. https://doi.org/10.1021/acsmedchemlett.1c00425.

(24) Porter, N. J.; Osko, J. D.; Diedrich, D.; Kurz, T.; Hooker, J. M.; Hansen, F. K.; Christianson, D. W. Histone Deacetylase 6-Selective Inhibitors and the Influence of Capping Groups on Hydroxamate-Zinc Denticity. *J. Med. Chem.* **2018**, *61* (17), 8054–8060. https://doi.org/10.1021/acs.jmedchem.8b01013.

(25) Porter, N. J.; Mahendran, A.; Breslow, R.; Christianson, D. W. Unusual Zinc-Binding Mode of HDAC6-Selective Hydroxamate Inhibitors. *Proc. Natl. Acad. Sci. U.S.A.* **2017**, *114* (51), 13459–13464. https://doi.org/10.1073/pnas.1718823114.

(26) Kalac, M.; Scotto, L.; Marchi, E.; Amengual, J.; Seshan, V. E.; Bhagat, G.; Ulahannan, N.; Leshchenko, V. V.; Temkin, A. M.; Parekh, S.; Tycko, B.; O'Connor, O. A. HDAC Inhibitors and Decitabine Are Highly Synergistic and Associated with Unique Gene-Expression and Epigenetic Profiles in Models of DLBCL. *Blood* **2011**, *118* (20), 5506–5516. https://doi.org/10.1182/blood-2011-02-336891.

(27) Blagitko-Dorfs, N.; Schlosser, P.; Greve, G.; Pfeifer, D.; Meier, R.; Baude, A.; Brocks, D.; Plass, C.; Lübbert, M. Combination Treatment of Acute Myeloid Leukemia Cells with DNMT and HDAC Inhibitors: Predominant Synergistic Gene Downregulation Associated with Gene Body Demethylation. *Leukemia* **2019**, *33* (4), 945–956. https://doi.org/10.1038/s41375-018-0293-8.

(28) Moufarrij, S.; Srivastava, A.; Gomez, S.; Hadley, M.; Palmer, E.; Austin, P. T.; Chisholm, S.; Diab, N.; Roche, K.; Yu, A.; Li, J.; Zhu, W.; Lopez-Acevedo, M.; Villagra, A.; Chiappinelli, K. B. Combining DNMT and HDAC6 Inhibitors Increases Anti-Tumor Immune Signaling and Decreases Tumor Burden in Ovarian Cancer. *Sci. Rep.* **2020**, *10* (1), 3470. https://doi.org/10.1038/s41598-020-60409-4.

(29) Ianevski, A.; He, L.; Aittokallio, T.; Tang, J. SynergyFinder: A Web Application for Analyzing Drug Combination Dose–Response Matrix Data. *Bioinformatics* **2017**, *33* (15), 2413–2415. https://doi.org/10.1093/bioinformatics/btx162.

(30) Sun, X.; Qiu, J.; Stout, A. Compounds as S-nitrosoglutathione reductase inhibitors. WO 2012/170371 A1, 2012.

(31) Molecular operating environment (MOE), 2022.02. Montreal: Chemical Computing Group ULC; **2022**.

(32) Jones, G.; Willett, P.; Glen, R. C.; Leach, A. R.; Taylor, R. Development and Validation of a Genetic Algorithm for Flexible Docking 1 1Edited by F. E. Cohen. *J. Mol. Biol.* **1997**, *267* (3), 727–748. https://doi.org/10.1006/jmbi.1996.0897.

(33) Schäker-Hübner, L.; Warstat, R.; Ahlert, H.; Mishra, P.; Kraft, F. B.; Schliehe-Diecks, J.; Schöler, A.; Borkhardt, A.; Breit, B.; Bhatia, S.; Hügle, M.; Günther, S.; Hansen, F. K. 4-Acyl Pyrrole Capped HDAC Inhibitors: A New Scaffold for Hybrid Inhibitors of BET Proteins and Histone Deacetylases as Antileukemia Drug Leads. *J. Med. Chem.* **2021**, *64* (19), 14620–14646. https://doi.org/10.1021/acs.jmedchem.1c01119.

(34) Kraft, F. B.; Hanl, M.; Feller, F.; Schäker-Hübner, L.; Hansen, F. K. Photocaged Histone

Deacetylase Inhibitors as Prodrugs in Targeted Cancer Therapy. *Pharmaceuticals* **2023**, *16* (3), 356. https://doi.org/10.3390/ph16030356.